Printed polymers, patterned paper

Salentijn, Gert

CHAPTER III

PROCEDURES, MATERIALS AND APPLICATIONS FOR 3D PRINTING BY FUSED DEPOSITION MODELING FOR LAB-ON-A-CHIP

Abstract

In this work, the use of fused deposition modeling (FDM) in a microfluidics/lab-on-a-chip research laboratory is described. First, the specifications of this 3D printing method that are important for the fabrication of microdevices were characterized for a benchtop FDM printer. These include resolution, surface roughness, leakage, transparency, material deformation and the possibilities for integration of other materials. Next, the autofluorescence, solvent compatibility and biocompatibility of 12 representative FDM materials were tested and evaluated. Finally, we demonstrate the feasibility of FDM in a number of important applications. In particular, we consider rapid prototyping and the fabrication of fluidic channels, masters for polymer replication, and tools for the production of paper microfluidic devices. This work thus provides a guideline for (i) the use of FDM technology, by addressing its possibilities and current limitations, (ii) material selection for FDM, based on solvent compatibility and biocompatibility, and (iii) application of FDM technology to microfluidics/lab-on-a-chip research by demonstrating a broad range of illustrative examples.

Accepted – Analytical Chemistry **2017**

Authors: G.IJ. Salentijn[1,2], P.E. Oomen[1], M. Grajewski[1], and E. Verpoorte[1]

[1] Pharmaceutical Analysis, Groningen Research Institute of Pharmacy, University of Groningen, THE NETHERLANDS
[2] TI-COAST, Science Park 904, 1098 XH Amsterdam, THE NETHERLANDS

3.1) Introduction

It is safe to say that scientists working in research laboratories are generally not self-sufficient when it comes to conducting experiments, regardless of the field of interest. For example, we all are dependent on external suppliers for consumables and labware, which in turn means that these materials must be ordered periodically and in a timely fashion, often in bulk, and stored somewhere before use. If experiments involve lab-on-a-chip technology and instrumental techniques, we must often turn to a workshop when it comes to things like customizing a microscope stage (for positioning a lab-chip, for example), or having clamping devices or alignment tools made. And if the workshop is busy (as they often are), our experiment is delayed. Resorting to temporary solutions like duct tape to align and fix components to do that experiment anyway generally just leads to additional delay. The iterative development of a lab-chip device using "rapid" prototyping approaches can slow down significantly too, if we are dependent on external partners or companies to perform certain processing steps. All these are recurring issues, or annoyances at the very least, to which we have often had to resign ourselves in the prototypical microfluidics lab. The bigger problem is, of course, that these inconveniences cause us to be inefficient against our will, meaning they cost time and money. Can we envision a world where we can shed our experimental dependence on these kinds of external factors? Perhaps we can – at least, if we can master the new additive manufacturing techniques that constitute 3D printing.

3D printing is not a new technology, as it has been used in some industrial settings for over thirty years. However, 3D printing systems have tended to be very specialized and expensive up until recently, making them relatively inaccessible for a broader spectrum of potential end-users. In addition, early equipment was often not very user-friendly, with long and relatively unreliable printing processes being typical. The history of 3D printing, as well as a comparative description of a number of different 3D printing approaches, has been nicely summarized in recent reviews[1–3].

In the last few years, we have seen a rapid increase in publications on the use of 3D printing in bio-analytical and microfluidics research[2]. It has been used for the fabrication of channels[4–8], sample cartridges[9], and molds for replication of channels in poly(dimethylsiloxane) (PDMS)[10–13]; hydrophobic patterning in paper microfluidics[14]; and fabrication of labware and customized setups[15–22]. Furthermore, 3D-printed materials have been studied to some extent with respect to their physical properties[6,23] and biocompatibility in cell or tissue-based assays[15,18,22,24]. As optical transparency is often a problem with 3D-printed lab-chip devices, incorporation of glass slides into these devices has also been reported[22,24]. These advances have been achieved with different 3D printing approaches, namely stereo lithography (SL), fused deposition modeling (FDM), inkjet 3D printing, digital light processing (DLP), and selective laser sintering (SLS). This means that the experience that lab-on-a-chip researchers have with 3D printing is somewhat fragmented. It would therefore be useful to assess and

characterize all these approaches individually, to allow for a better comparison of approaches and selection of the most suitable approach for a given application.

As a first step in this direction, we focus in this contribution on 3D printing by FDM . We describe the technology and address its current possibilities and limitations with respect to lab-on-a-chip devices, and more generally, experimental research. Furthermore, this work contains an extensive table in which several important properties (including biocompatibility and solvent compatibility) of twelve representative FDM materials are listed, to aid in material selection for specific medical, biological, or chemical applications. Finally, we demonstrate the applicability of FDM to the fabrication of (bio)analytical microdevices and customization of experimental setups. All the examples in this paper were designed, fabricated and implemented in our lab at the University of Groningen, and are presented here to show the impact that 3D printing has had on our own "micro-environment".

3.2) Fused Deposition Modeling (FDM)

FDM is based on the melting and extrusion of polymer filament. Filament is fed into and melted in a heated metal cylinder ending in a nozzle. As fresh filament is supplied continuously into this component, the molten polymer is pushed out of the nozzle, forming a polymer thread roughly the size of the nozzle diameter. In order to shape this thread into a plastic part, the nozzle is placed above a metal plate (*print bed*) at a distance that depends on the desired resolution. Upon exiting the nozzle, the filament is deposited on this print bed, which can be heated in order to promote attachment. When the print bed and nozzle are both controllably moved in perpendicular directions, we can draw a two-dimensional figure on the print bed, having the thickness of one polymer thread. This thickness (generally between 0.1 and 0.3 mm) is controlled by (i) the distance between the nozzle and the print bed and (ii) the ratio between the flow rate of filament through the nozzle and the printing speed. When the first layer is finished, the print bed is lowered by a fixed distance (*i.e.* the thickness of a single layer) and a second layer can be printed on top of the original one. By repeating these steps, an object is created in an additive manner.

In order to print a 3D-drawn model, it first needs to be translated to a file which guides printer operation. This process is described in detail by Gross and co-workers[1]. In short, the 3D drawing (often a vector file) is saved in the *.STL format, which is a triangular surface mesh. This file is then sliced into a path for the extruder to follow (generating a G-code); the solid model is thus converted into a digital equivalent of filament threads.

3.3) Materials and Methods

3.3.1) Characterization of a benchtop FDM printer

For the fabrication of the devices in this work, a Felix v.3.0 (FELIX printers, de Meern, The Netherlands, nozzle diameter = 0.35 mm) was used. This FDM printer was chosen because of

its open and accessible architecture. SolidWorks (Waltham, MA, USA) was used to design the 3D models for printing, which were then sliced using sFact/Skeinforge freeware. Repertier host freeware was used to control the 3D printer.

3.3.1.1) Characterization of resolution, surface roughness and overhang

Embedded channels (rectangular, circular and diamond-shaped) were printed in red PLA (EasyFil, Formfutura, Nijmegen, The Netherlands) with dimensions ranging from 0.1 to 5.0 mm with an aspect ratio of 1 (Figure S3.1, Supplementary Information (SI)). The structures were illuminated from both sides to visualize the surface and the channel under a microscope (Leica S8APO, Leica Microsystems, Wetzlar, Germany). Slice and print settings are listed in Table S3.1, SI.

3.3.1.2) Prevention of leakage

An embedded channel (l = 15 mm, w = 0.8 mm, h = 0.8 mm) with an inlet and outlet reservoir (ID = 4 mm) was printed in Transparent PLA (Figure S3.2A, ESI). The part was printed with different *infill solidities* and *shell numbers* (Table S3.1, Figure S3.2B, SI). The value of the *infill solidity* parameter determines the ratio between filament and air in the interior of the part; a value of 0.2 yields a very open infill, whereas 1.0 leads to a complete fill of the internal volume. *Shell number* refers to the number of adjacent filament threads that outline the contours of all structures. After the parts were printed, 50 µL of a methanol/water solution (1:1 (v/v)) of blue food dye (Jo-La, E131, Bharmco Foods, Braambrugge, The Netherlands) was introduced to the inlet reservoirs to fill the channels, and photographs were taken.

3.3.1.3) Transparency

A device was designed with an internal cavity that acted as a frame for a glass microscope slide (Table S3.1, Figure S3.3, SI) and printed in Transparent PLA. Once the device had been printed up to the point where the cavity walls were completed, the print was paused, and the glass slide was inserted into the cavity. The print was then continued, and sealed channels were printed on top of the glass slide (*i.e.* the glass slide served as the bottom of the channel). Once finished, the channels were filled with aqueous blue dye solution and imaged from the top and bottom through the PLA and glass layers, respectively. The transparency of the PLA device could be characterized qualitatively in this way.

3.3.2) Polymers for FDM printing

A number of physical and biological specifications of twelve FDM filament materials were assessed in this study. The materials with their respective printing parameters are listed in Table S3.2, SI. These 12 materials are representative of materials which are commercially available for FDM. They comprise different polymers, and have varying degrees of elasticity.

3.3.2.1) Autofluorescence

The autofluorescence of a material refers to its own tendency to emit fluorescence upon illumination with light at certain wavelengths. The autofluorescence of each material was evaluated under an inverted fluorescence microscope (DM-IL, Leica Microsystems, Wetzlar, Germany) equipped with a Leica DFC300 FX camera (Leica Microsystems, Wetzlar, Germany), for three different wavelength ranges. Y3 ET (ex/em 530-557/575-647 nm), GFP ET (ex/em 450-488/505-545 nm) and CFP ET (ex/em 430-445/460-500 nm) filter cubes were used. Photographs were acquired with an acquisition time of 50 milliseconds. The average color intensity of the photographs was measured using ImageJ[25]. The autofluorescence of the materials was classified based on the intensity data.

3.3.2.2) Solvent compatibility

Test structures were printed with all twelve materials to assess their compatibility with water, methanol, acetonitrile, isopropanol and acetone. The test structure was a 2D generic human figure, selected because it combines relatively thick (torso, approximately 5 mm) and thin (limbs, approximately 1 mm) features in one structure. Fifteen structures were produced per material (3 per solvent tested, one each for exposure times of 1 hour, 24 hours, and 168 hours). The dissolved weight and the remaining weight of each figure were determined after exposure, and post-exposure photographs were acquired (see Protocol S3.1, SI). The materials were classified according to the criteria in Table S3.3, SI.

3.3.2.3) Biocompatibility

Biocompatibility in the context of this study refers to the material property that results in the viability of cells and tissue being unaffected when exposed to the material under culture conditions. Conversely, a material that is not biocompatible will adversely affect cell or tissue viability in its proximity to some extent, resulting in altered cell behavior or even death.

Cell model: Human Umbilical Vein Endothelial Cells (HUVEC) were selected because of their high sensitivity to changes in culture conditions and broad application in studies of drug mechanisms, wound healing, immune response, oxidative stress, and arteriosclerosis[26]. They constitute a more sensitive and representative model for biocompatibility studies than immortalized cell lines. The preparation and cultivation of HUVEC is described in detail in protocol S3.2, SI.

Tissue model: To study the possible effects of the printed materials on incubated tissue, precision-cut liver slices (PCLS; Wistar rats) were chosen as a model. The prepared PCLS have a diameter of 5 mm and a thickness of about 200 µm[27]. The use of these dimensions ensures that the slice contains several functional liver units and therefore serves as a good representative for the entire organ. All experiments were approved by the Animal Ethical

Committee of the University of Groningen. The preparation and cultivation of PCLS are described in detail in protocol S3.2, SI.

Exposure procedure: Exposure experiments on both cell and tissue models were performed in 12-well plates.

HUVEC: When HUVEC cultures achieved 60-80% confluency, generally after an overnight cultivation, 3D-printed rings (ID 17 mm; OD 21 mm, thickness 1 mm) were placed in the wells after refreshing the medium. In addition, HUVEC without exposure to 3D-printed materials were included in the experiment as positive controls. Wells filled with medium were included as negative controls. The HUVEC were cultured for 18h with the FDM materials (37°C; 95% air, 5% CO_2). The viability of the cultures was assessed using an MTT assay, supported by visual inspection of the cell layers.

PCLS: After pre-incubation, which was performed post-slicing in order to remove cell debris and allow restoration of function, the PCLS were transferred to a new well containing a 3D-printed ring and fresh, pre-warmed medium. A 24-h slice-incubation period followed at 37°C, 80% O_2 and 5% CO_2. In addition, PCLS without exposure to 3D-printed materials were included in the experiment as positive controls. The viability of the slices was assessed using a fluorescence-based assay for lactate dehydrogenase (LDH) leakage into the medium, and a luminescence-based assay for the adenosine triphosphate (ATP) content of the slices. For the LDH analysis, a control experiment was performed to assess the possible influence of the 3D-printed polymer rings on the assay itself. All three assays are described in detail in Protocol S3.2, SI.

Data analysis: Three different rat livers and three different batches of HUVEC were used for the experiments, using triplicates for each material (n = 3). Outliers were removed based on both statistical analysis (Grubbs test) and visual inspection of the data (boxplots). After these were removed, R software (v. 3.02, Vienna, Austria) was used to perform ANOVA with a post-hoc Tukey's honest significance test to identify significantly different means in all viability assays. A p-value of ≤ 0.05 was considered as indicative of a significant difference. If no significant difference in assay outcome was observed compared to the relevant control experiment, the classification 'biocompatible (+)' was assigned. A significantly different outcome led to a classification of 'not biocompatible (-)'.

3.3.3) Applications of FDM printing

3.3.3.1) 3D-printed masters for PDMS replication

Two different negative masters for PDMS replication were 3D printed in red PLA. The slice and print parameters can be found in Table S3.1, SI. The first master was used to replicate straight channels in PDMS with an aspect ratio of 1 (height = width). Structures were 15 mm long, and the widths and heights were varied between 0.3 and 5.0 mm. The second master

contained a single, complex channel (0.15 mm height, 0.3 mm width). PDMS replication and device fabrication are described in Protocol S3.3, SI. The channels were filled with a solution of blue dye dissolved in water/methanol (1:1 (v/v)) for visualization.

3.3.3.2) Hydrophobic patterning of paper with wax using 3D-printed tools

Hydrophilic channels or lanes can be defined in paper using hydrophobic patterning techniques. Passive fluid transport by capillary action then serves to move liquids through the paper channels to carry out reactions or other sample handling. Hydrophobic patterning may be accomplished in different ways. One approach which has received some attention in our lab involves the use of wax deposition. A 3D-printed tool was used for the wax-dipping method, as published by Songjaroen *et al*.[28] The tool consists of 3 parts, as shown in the SI, Figure S3.4. The base of the tool with (1) a handle, (2) holes for screws and (3) one smooth surface was 3D printed in PLA (SI, Figure S3.4A). The smooth surface on the first printed layer was obtained by minimizing the distance between the print bed and the nozzle to below 100 µm, which led to better spreading of deposited polymer on the print bed and thus a smooth surface. A mask for wax patterning was 3D printed in PLA as well (SI, Figure S3.4B). This mask was designed to shield specific regions from wax deposition, so that they would remain hydrophilic. Chromatography paper was placed between the base and the mask. A third PLA structure was printed and placed on top of the assembly to provide additional pressure on the mask centrally (SI, Figure S3.4C). The total assembly was screwed together tightly.

Paraffin wax (Sigma Aldrich, Steinheim, Germany) was melted in a beaker on a hotplate set to 120°C. The assembled tool with the paper was dipped in the molten wax for approximately one second, after which the assembly was withdrawn from the wax and the paper subsequently removed from the assembly. Excess wax on the paper was removed with a scalpel. Four masks with different hydrophilic channel widths (0.5, 1.0, 1.5, 2.0 mm) were used to produce paper microfluidic structures (n = 5 per mask), which were then photographed under the microscope with a ruler for size calibration. The channel width was determined with ImageJ[25].

3.4) Results and discussion

3.4.1) Characterization of a benchtop FDM printer

3.4.1.1) Resolution, surface roughness and overhang

Resolution is an important issue with respect to the current generation of benchtop 3D printers if small (<100 µm) channels are desired. Most published examples of 3D-printed microchannels report channel sizes of a few hundred µm (*e.g.* 200-250 µm for DLP[6,7,29]). Figure 3.1 shows the resolution that was achieved with our benchtop FDM printer, and whether channels were sealed or had collapsed during the printing process. Open channels

with dimensions below 200 µm (0.4 mm by design) were obtained, which was ascertained by shining light through them. The difference between the actual and designed channel width is a result of the tolerances of the printer. Positive structures (solid, protruding) are generally printed slightly larger, whereas negative structures (recessed, open/embedded) are slightly smaller. The surface and shape of these small channels are not so smooth, due to the fact that these dimensions are in the same range as the dimensions of a single thread of extruded material. Larger channels assume a more well-defined shape.

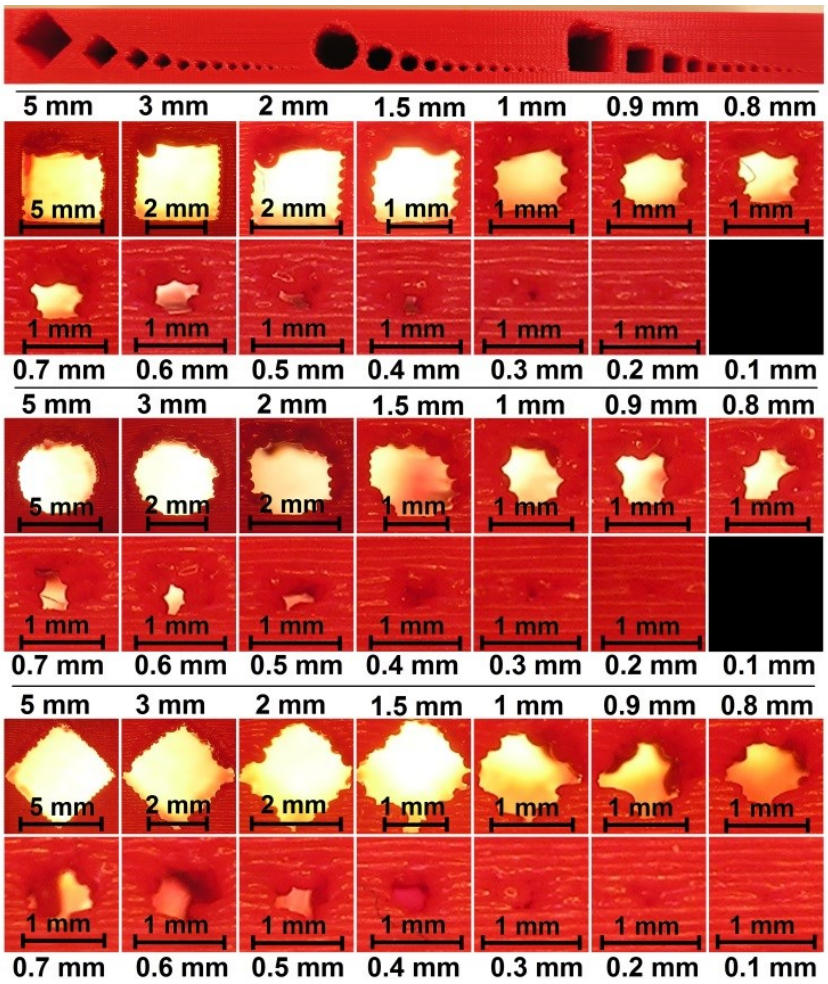

Figure 3.1: Resolution of FDM printed channels (rectangular, circular and diamond-shaped). The top panel shows the front view of the entire test structure, presented in Figure S3.1, SI. The panels below depict enlarged views of the individual channels, all scaled individually to the size of the frame.

In other work on FDM, a channel with a diameter of 0.8 mm was successfully used in 3D-printed reaction ware[4]. However, the effect of limited resolution due to filament dimension is clearly visible in Figure 3.1 at this smaller scale. In larger channels, the microstructure of the fused threads of filament is identical to that of smaller channels, which means that these channels possess the same absolute surface roughness. However, the overall effect of individual filaments on the definition of channel shape is much less pronounced, as can also

be seen in Fig. 1. This is inherent to the FDM printing process. It is possible to chemically smooth ABS and PLA parts with acetone and ethyl acetate vapors, respectively. In this process, the surface of a part is dissolved and thus the roughness of the surface decreases. Surface smoothing with vapor has a trade-off, however, as small structures also tend to be smoothed, leading to substantial loss of their definition. Moreover, the process is difficult to control, especially for smaller features. For small channels, smoothing is therefore not a realistic option. Smoothing of a surface for better sealing or fabrication of labware could be beneficial for the final product. This was not investigated in this study.

Figure 3.1 also shows the quality of overhanging structures. Due to the nature of FDM, bridging structures are difficult to produce, as there are no layers supporting them. One solution to this problem is to print support structures (implemented into the G-code during slicing), which can be removed afterwards. However, such structures are impossible to remove inside small channels. A second option is to use dual-head printing, in which the channel can be filled with a water-soluble material (*e.g.* PVA). The easiest solution (if applicable) is to use designs which circumvent this issue altogether. Overhang tends to start collapsing when its size exceeds a certain threshold. Below this threshold (more or less 1 mm, see Figure 3.1), overhang collapse is not a problem. If a circular or diamond channel shape is chosen instead of a rectangular one, the overhang is gradually formed. Figure 1 shows that the quality of the cross-sectional geometry of large channels increases as we go from rectangle (in this case, square) to circle to diamond. However, for channels 1 mm or smaller, the fidelity of the cross-sectional geometry is best for the rectangular shape.

3.4.1.2) Prevention of leakage

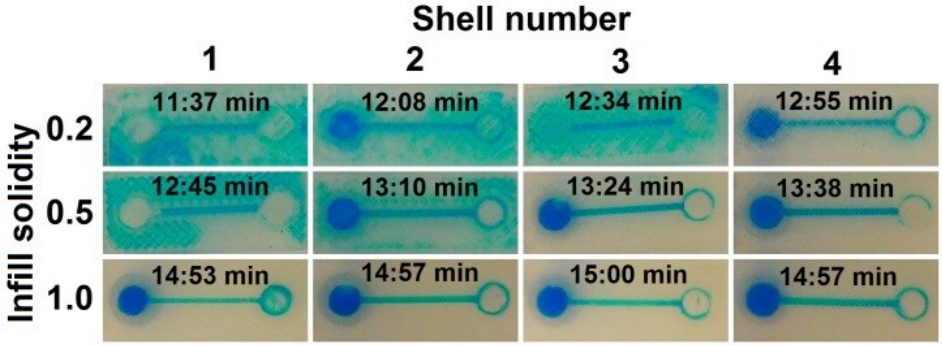

Figure 3.2: Influence of infill solidity and shell number on leakage prevention in a 3D-printed channel. Estimated print time (after slicing) is shown for each setting as well. Detailed schematic diagrams are given in Figure S3.2, SI.

Leakage is probably the most undesirable phenomenon that a fluidic device can exhibit. Figure 3.2 demonstrates a number of channels (width x height = 0.8 x 0.8 mm) of the exact same geometry, yet sliced with different settings. This figure shows that a more solid infill is preferential for fluidic devices. However, this means a larger consumption of material, as well as increased printing times, as can be seen from the estimated print times, calculated by the

software after slicing. Another way to prevent leakage is to increase the shell number. Even with a very open infill (0.2), a shell number of '4' led to a channel which did not exhibit leakage into the rest of the part. These settings also result in shorter print jobs, than with the high-infill settings.

3.4.1.3) Transparency

Many microfluidic devices rely on visual (microscopic) inspection for control of their operation. For this reason, materials such as PDMS, glass and transparent thermoplastics are very popular in the field. Transparency is claimed for a number of FDM materials. As of yet, to the best of our knowledge, 60% transmission (430-620 nm light) through a 500-µm-thick polymer layer is the highest level of transparency achieved, but this was done with photocurable resin and DLP[6].

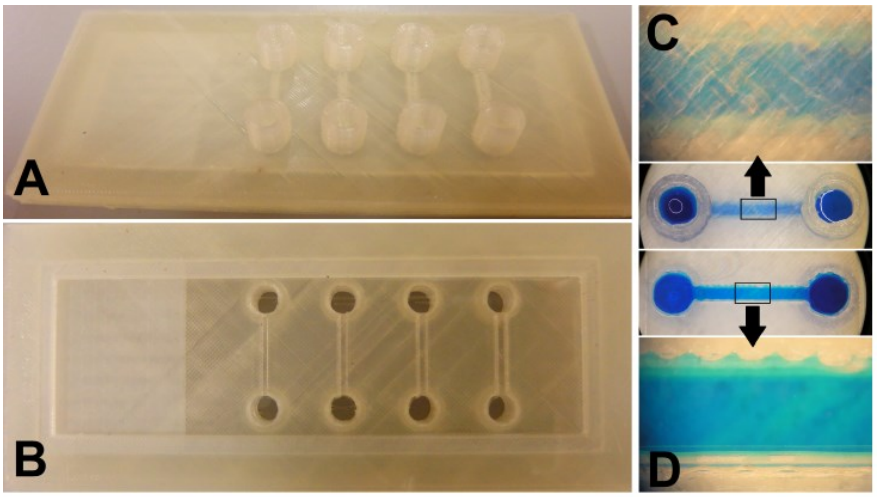

Figure 3.3: (A, B) PLA-glass device with sealed fluidic channels, suitable for microscopic inspection (see SI, Figure S3.3 for dimensions). The glass slide is incorporated into a single 3D-printed PLA part. The glass is inserted during the print, by pausing the print. (C) Transparent PLA was used, which gives semi-transparency through a limited thickness. The thickness of the top PLA layer through which the blue solution is being visualized is 0.8 mm, which is clearly too thick for a clear image of the microchannel (1 mm wide and high). (D) The blue solution in the same printed channel can be clearly imaged under the microscope when viewed through the glass bottom. There appears to be a bit of leakage along the edges of the PLA channel where it contacts the glass slide.

In FDM, not only the transmission of the material itself, but also the microstructure of the produced parts is relevant. Due to the stacking of layers of threads, light is scattered as it passes through a polymer device. When using one of these "transparent" materials, see-through devices can be made, as long as the thickness of the part is kept at a minimum (roughly up to 1 mm). In order to cope with this, glass slides can be integrated into 3D-printed devices. One possible approach is to fabricate a channel with the 3D printer which is open at the bottom, and then attach it with glue, or a photocurable resin to the glass slide[22,24]. To demonstrate the above, a test device with sealed channels was 3D-printed on top of an

embedded glass slide. Our approach underlines one attractive feature of FDM printing, as opposed to SL or DLP approaches: it is easy to integrate additional objects into 3D-printed structures during the print. Figure 3.3 shows this device, filled with an aqueous solution of blue dye, from the top (Figure 3.3A, PLA side) and from below (Figure 3.3B, glass side). The thickness of the PLA ceiling over the channel is 0.8 mm. Although the liquid can be observed when the channel is viewed from above (Figure 3.3C), it is clear that true transparency is not achieved. However, when viewed through the glass slide at the bottom of the channel we obtained an unobscured view. The obtained channels can confine aqueous solutions and are compatible with microscopy on the glass-slide side. More research is required, however, to quantify and improve the strength of PLA adhesion to the glass, which is weaker than attachment to PLA. When PLA is printed on top of PLA, the layers melt together, which does not happen when printed on glass. Noteworthy is that FDM provides for the incorporation of other materials or components besides glass, such as paper, membranes, and electrodes.

3.4.1.4) Combining materials

In addition to the integration of non-3D-printed objects into a part, FDM also allows the fabrication of hybrid devices. The most complex structures can be obtained by using dual-head printing, in which two materials can be printed more or less simultaneously, thus allowing embedding of one material in the other. A simpler approach is to pause the print at a certain point and exchange the filament. One such example can be found in the combination of PLA with Arnitel in a two-layer part for masking paper during exposure to oxygen plasma[14].When pressure is applied to the rigid PLA side, the flexible Arnitel side conforms to whatever surface it is in contact with, in this case paper. Using this approach, it was possible to shield paper from exposure to oxygen plasma, as demonstrated in previous work[14].

3.4.1.5) Warping

During a print, especially for large, time-consuming parts, the internal temperature of the object being printed tends to vary. Materials are printed at high temperature (around 200°C, the temperature of the extrusion nozzle) onto the print bed (around 60°C) and cooled with an integrated fan for quick solidification. This usually causes shrinkage and can lead to deformation through warping. Warping can lead to detachment from the print bed and thus compromises part fabrication. Warping can easily become a problem if the temperature of the print bed is too low, or if the print bed is not well aligned or is too far from the extruder. Under all these circumstances, the initial attachment to the print bed is insufficient. Materials that require higher temperatures for extrusion and bed adhesion are especially prone to warping and detachment (*e.g.* ABS). There are a number of options to reduce or prevent part detachment due to warping: (i) place the printer in a closed box (which prevents convective air movement) that can be heated to maintain a more uniform temperature distribution, (ii) coat the print bed with a material that enhances adhesion (*e.g.* ABS dissolved in acetone or hairspray), (iii) print the first few layers of the part in a material that has good adhesion to the

plate (*e.g.* PLA soft) and then switch to the actual material for the print, (iv) have the slicing software include a brim in the G-code for the part, which can be removed after the print is done. Incorporating a brim means that a number of additional shells are printed on the first layer to increase the surface attached to the plate.

3.4.2) Polymers for 3D printing

The results for the different characterizations performed on 12 FDM materials can be found in Table 3.1. We refer the reader to Table S3.2 for a list of the printing parameters for these materials. The following sections deal with the different aspects of the materials that need to be taken into account when a material is selected for an application. Note that suppliers of filament (i) generally do not list the exact chemical composition of their filament and (ii) are continuously improving their products, as we are currently going through a phase of rapid development in the 3D printing field.

3.4.2.1) Polymer printability

This section describes the problems that might be encountered when printing the different polymers individually. The success or failure of the print process for a part largely depends on whether the first layer is printed properly or not, as discussed above. Some of the problems that might occur at the beginning of the printing process are material-specific, often related to warping phenomena. As alluded to in the previous section, warping and/or detachment from the print bed is an important cause for failure. The print bed used in this work can reach a maximum temperature of approximately 80°C. This means that materials like ABS, PS, and especially PC are difficult to print, as they require higher temperatures for bed adhesion. In other words, these materials are more prone to warping. For small parts, this can be overcome by printing with a brim, as discussed above. Coating of the print bed with adhesive material also improves attachment, but was not an option for this study, as it would lead to contamination of the test structures. For the production of PC parts, another temperature-related problem can be encountered, associated with the actual softening of printer components (*e.g.* PEEK insulation) after prolonged usage at temperatures around 250°C. This can lead to irreparable damage of the printer component.

3.4.2.2) Autofluorescence

Autofluorescence can be a limitation when the material is used in tests that rely on fluorescence, especially for quantitative analysis. Table 3.1 shows to which extend the 12 materials that were tested exhibit autofluorescence at different wavelengths. We defined categories with selected thresholds and classified the materials accordingly. The photographs and numerical data can be found in Figures S3.5 and S3.6 of the SI, respectively. All the materials tested exhibit autofluorescence to some degree, but with some the level is quite acceptable. PLA 45 can be employed when green and red fluorescence are used, whereas PLA soft is applicable to blue and red. In general, the FDM materials tested exhibited less

autofluorescence at red wavelengths. The application of fluorescence detection at longer visible (red) wavelengths in a 3D-printed device thus allows for a broader selection of FDM materials. Importantly, some of the tested materials contain (colored) additives, which might influence the level of autofluorescence.

Table 3.1: Solvent compatibility, biocompatibility and autofluorescence of 12 FDM materials*

Material	Composition based on	Color	Transparency	Autofluorescence blue	Autofluorescence green	Autofluorescence red	Water compatible	Methanol compatible	Acetonitrile compatible	Isopropanol compatible	Acetone compatible	HUVEC compatible	PCLS compatible
PLA gold	Polylactic acid	Gold	None	+	++	+	+	+/-	--	+	--	+	+
Transparent PLA	Polylactic acid	Colorless	Semi	+	+	+/-	+	+/-	--	+	--	+	+
PLA soft	Polylactic acid	Beige	None	+/-	+	+/-	+	+	+/-	+	+/-	+	+
PLA 45	Polylactic acid	White	None	++	+/-	-	+	+/-	--	+/-	--	+	+
ABS	Acrylnitrile butadiene styrene	Orange	None	++	++	++	+	-	--	+	--	+	+
PC	Polycarbonate	Colorless	Semi	++	++	++	+	+	-	+	-	+	+
PS	Polystyrene	Crème	None	++	++	+	+	+	+	+	--	+	+
PVA	Poly vinyl alcohol	Light yellow	Semi	++	++	++	--	--	-	-	--	-	-
PET	Polyethylene terephthalate	Colorless	Semi	++	+	+/-	+	+	-	+	-	+	+
T-Glase	Polyethylene terephthalate	Colorless	Semi	++	+	+/-	+	+	-	+	-	+	+
Arnitel	Thermoplastic Co-Polyester	White	None	++	++	+/-	+	+	+	+	+	+	+
Bendlay	Acrylnitrile butadiene	Colorless	Semi	+	++	+	+	+	-	+	-	+	+

* The classification of biocompatibility, solvent compatbility and autofluorescence is based on the rules for performance described in the Materials and Methods section (Biocompatibility section, Data Analysis) and in the SI (Protocol S3.1, Solvent compatibility; Figure S3.6, Autofluorescence).

3.4.2.3) Solvent compatibility

Table 3.1 gives an overview of the compatibility of the 12 materials with 5 different solvents. Again, the materials were classified into different categories based on numerical data and photographs after one-week (168 h) exposure (respectively, Figures S3.7 and S3.8, SI). These results demonstrate that all the materials except PVA are compatible with water. Isopropanol

and methanol are both compatible with most materials, but acetonitrile and acetone are more challenging. Arnitel is the only material from this selection which can be employed for all five solvents. Furthermore, it is remarkable that the flexible materials (PLA soft and Bendlay) show better solvent compatibility that the rigid filament on which they are based (PLA and ABS, respectively), which we assume is caused at least in part by additives meant to increase flexibility. Finally, it should be noted that in a few cases the sum of dissolved weight and remaining weight exceed 100% of the initial weight (see Figure S3.7). This can potentially be attributed to swelling phenomena and/or encapsulation of solvent in the polymer matrix.

3.4.2.4) Biocompatibility

Table 3.1 shows the results of the biocompatibility studies with HUVEC and PCLS. A material was considered biocompatible if the test result was not found to be statistically different from the control experiment. Out of the twelve FDM materials tested, eleven show biocompatibility with HUVEC and PCLS (Figures S3.9-S3.13, SI); only PVA shows significant toxicity for both biological models in comparison with the controls ($p = 0.009$ for MTT test in HUVEC; $p=2*10^{-7}$ for LDH leakage in PCLS; $p=0.002$ for ATP measurement in PCLS). Although PVA is described as a biocompatible material and is used in medical studies[30], it was toxic in experiments performed with both HUVEC and PCLS. This may be explained by the high solubility of PVA in the aqueous medium. This leads to an observed increase in medium viscosity (medium becomes gel-like), which may result in decreased diffusion of nutrients and oxygen to the cells and hence decreased viability. Furthermore, contaminants or additives might be present in the filament. After dissolution these might have a toxic effect on the biological material. The fact that the solvent compatibility studies show no dissolution of any of the other materials in water is also in line with the observation that they do not cause a loss in viability in cells or tissue.

A control experiment was carried out to assess the possible influence of the materials on the fluorescence-based LDH assay. It measured absolute emission intensity, in the absence of PCLS. The only material that caused a significant increase of the intensity measured was PVA ($p=4 * 10^{-7}$). However, the average difference from the control was 134 AU, which is less than 1% of the average fluorescence intensity measured in medium for PCLS incubated with PVA for 24 hours. The effect of PVA itself on the LDH assay can therefore be regarded as negligible.

The assays show similar results in cell and tissue cultures. Futhermore, the results are comparable to those found in earlier studies to assess the biocompatibility of FDM materials[15,22,31] – though this study comprises a broader range of materials. To the best of our knowledge, we observe only one deviation from previous biocompatibility results, namely for ABS. Hyde and co-workers[15] found that ABS exhibits some toxicity toward human neuroblastoma cells and mouse pituitary cells. It was also shown that ABS influenced the functionality of cortical neurons. We however, have not observed any negative effects of ABS

on the HUVEC or PCLS models. Furthermore, the toxicity of a material might also be attributed to additives in the material, which can vary from producer to producer. While our results can serve as a guideline for selecting a safe material for cell or tissue studies, researchers in other labs and working with other cells or tissue will need to confirm the biocompatibility of their materials for their biological models.

3.4.3) Applications of FDM printing

3.4.3.1) Rapid prototyping

In order to demonstrate the rapid prototyping capabilities of FDM, we use the example of a 3D-printed cartridge for paper spray ionization[9], which is an ambient ionization method for mass spectrometry (MS). A piece of paper cut into a sharp tip serves as a porous substrate for the generation of electrospray. When a high electric field is applied between the wetted paper tip and the orifice of the mass spectrometer, the sample is nebulized from droplets formed at the sharp paper tip. We developed a cartridge containing a chamber for the tip to enable physical stability and easier alignment with the MS. By incorporation of a tip into the cartridge, rapid and continuous wetting from a solvent reservoir was ensured through wicking structures. The cartridge is a complex 3D-printed device, consisting of 3 different parts. The development of this cartridge was completed in approximately 6 months, in a series of iterative 'design-print-test-evaluate' cycles.

The initial design (Figure 3.4A) consisted of a solvent reservoir, connected via an open channel to the chamber for the paper tip, and openings for sample introduction and an electrode. The two parts had to be screwed together to be assembled, which proved difficult to do in a leakage-free manner. To overcome this, the solvent reservoir was relocated to exclusively the bottom cartridge (Figure 3.4B) and pillars were used to press down the paper to further minimize contact between the printed parts. However, solvent supply from the reservoir through an embedded channel to the paper tip chamber remained difficult to control. Therefore, a thin strip of paper extending from the rear of the paper tip (*hydrophilic wick*) was placed over a *suspended beam* and subsequently immersed into the solvent reservoir, thus connecting them (Figure 3.4C, E). This led to good control of the solvent flow, but slow wetting of the paper by capillary forces, a passive process. Additionally in this design iteration, the screw holes were replaced by a slide-and-click mechanism to close the cartridge. Notice how both the slots and the tabs are designed with a gradual slope to ensure good print quality. In the final design (Figure 3.4D), a *hydrophilic wick* is suspended over a beam, partially reaching into the solvent reservoir (Figure 3.4F) and *solvent guide structures* were placed on the lid above the wick to promote fast wetting of the tip. Notice that the suspended beam was designed as a part of the cartridge in Figure 3.4C, and as a separate part (gray) to be inserted into the cartridge in Figure 3.4D. This is because the distance that needed to be bridged by the beam increased significantly. Furthermore, a second hydrophilic wick was introduced, suspended over a cavity, which allowed slow, continuous solvent supply to the

tip. The channel for this latter wick (Fig 3.4D #7), as well as the channel in Figure 3.4C (#7), are embedded in a single part, which is a unique feature of 3D-printed parts. The entire design process was exclusively under our control, which resulted in short cycle times for design iterations, and enabled us to continuously increase the level of device sophistication with respect to solvent transport.

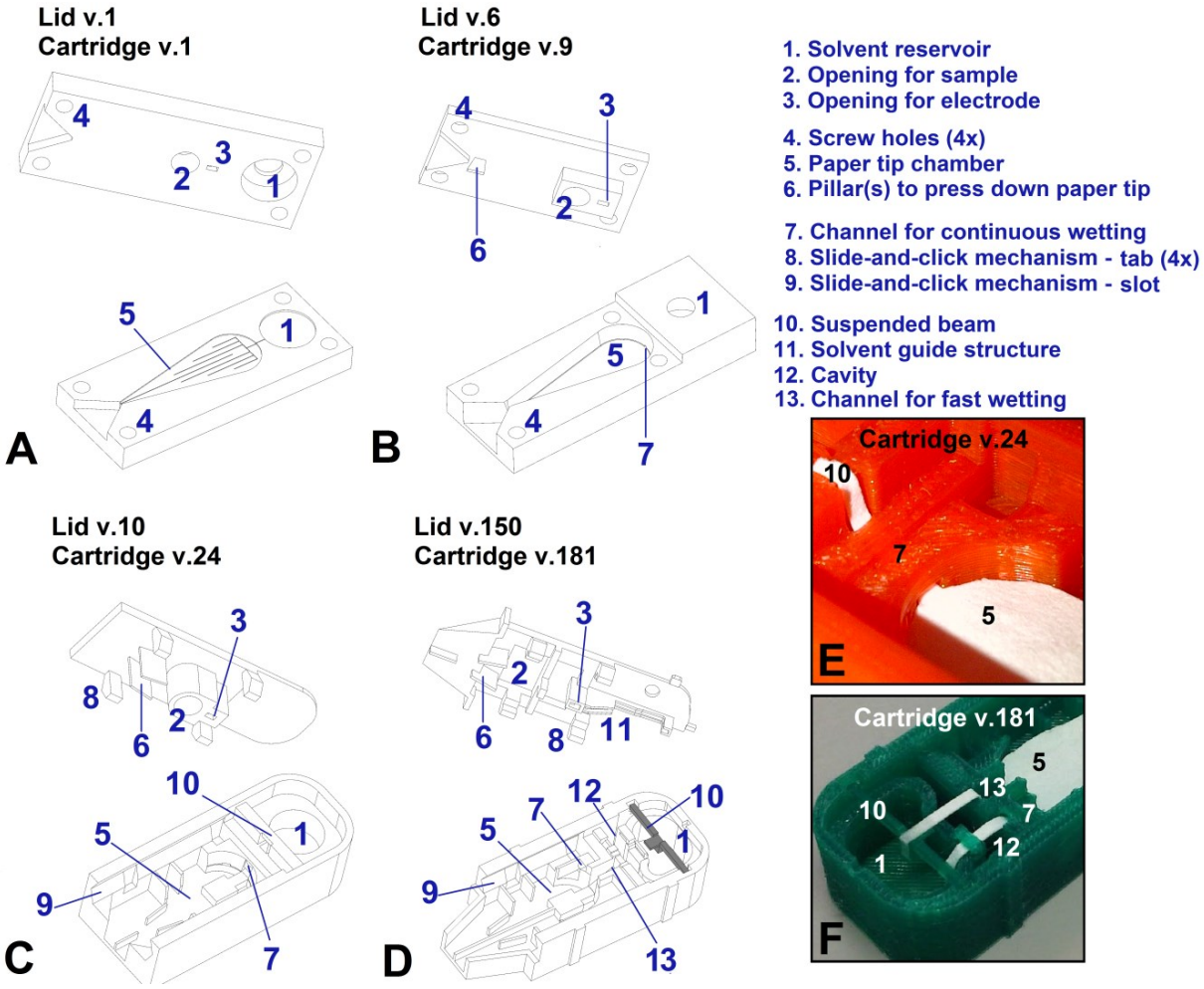

Figure 3.4: (A-D) Different stages in the rapid prototyping process of a paper spray ionization cartridge. (E-F) Photographs of two versions of the cartridge, which demonstrate positioning of the paper tip and hydrophilic wicks for solvent supply.

3.4.3.2) 3D-printed masters for PDMS casting

The use of 3D printers for the fabrication of masters which can be used for casting PDMS (and other curable materials) has been demonstrated for inkjet printing (down to 100 µm resolution[12]) and DLP (down to 50 µm resolution[10]). Figure 3.5 shows two FDM-printed masters and the resulting PDMS devices. The smallest channel produced had a width of approximately 300 µm. Figure 3.5 also demonstrates that complex architectures are easily achievable (Figure 3.5E), but that the variation in channel width in such devices is quite

substantial. The nominal width of the spirally laid out channel in Figure 3.5F, made using the master in Figure 3.5E, is 0.3 mm. However, the width of the dye-filled channel varies roughly between 0.1 mm and 0.5 mm. Additionally, the base plane of the master suffers from roughness, which is characteristic for FDM printing as discussed earlier. This is replicated in the PDMS cast, which can complicate bonding of the part to a flat surface for sealing. This in turn increases the likelihood of leakage. It is possible to use FDM-printed templates for PDMS replication, but other 3D printing methods are perhaps more suitable for this purpose, depending on the required resolution of the part.

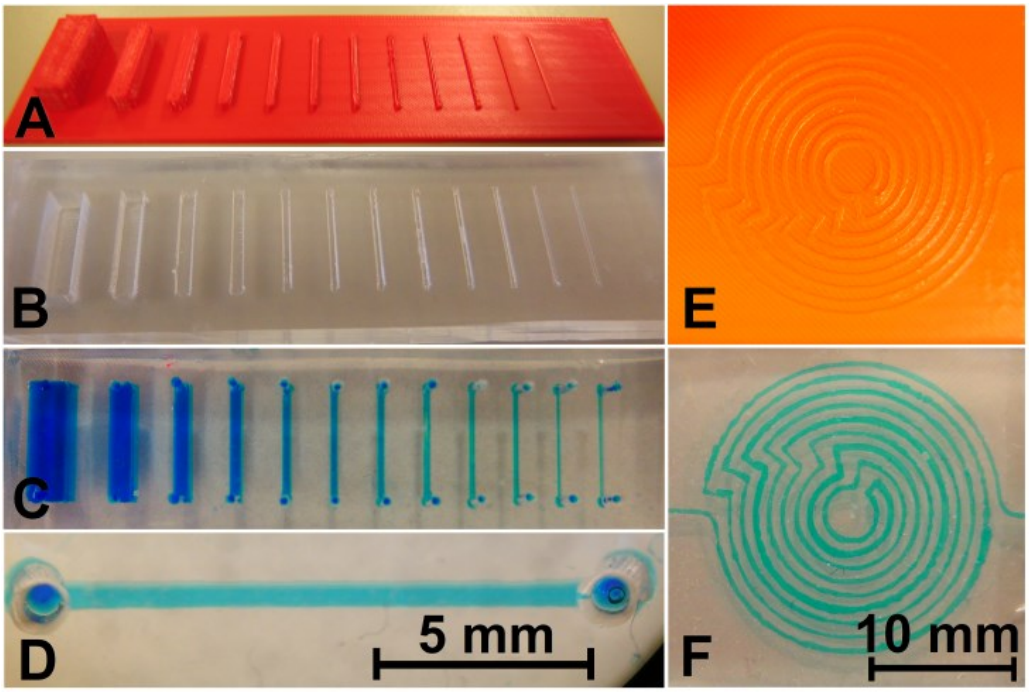

Figure 3.5: 3D-printed masters for PDMS casting. (A) Master for replication of straight channels (width and height varied between 0.3 and 5.0 mm, aspect ratio of 1). (B) PDMS replicate from the 3D-printed master. (C) Channels were sealed with a PDMS layer and filled with blue solution through holes lining up with the ends of the channel. (D) Expanded view of one of the filled channels. (E) Master for a complex channel. (F) PDMS replicate of the complex channel, filled with blue dye solution.

The production of sacrificial templates with 3D printing for replication of microfluidic devices (by dissolution of the polymer after curing) has been reported[32], and is a method that can be adapted for FDM. One could print a 3D object in PVA, cast PDMS around it and later dissolve the PVA in water to remove it. This approach could also circumvent the above-mentioned problem of leakages in the PDMS device due to surface roughness of the master, as the PDMS device could be replicated in a single step.

3.4.3.3) 3D-printed channels

Many reports have described the use of 3D-printed channels, some of which employed FDM[4]. Figures 3.1, 3.2 and 3.3 of this paper show simple examples of embedded channels made with

FDM as well. From an applications point-of-view, FDM printing is suitable for the production of fluidic channels. However, if one is aiming to produce channels with cross-sections on the order of 100 µm or less, FDM is currently not the way to go. This is because FDM resolution is limited by the nozzle diameter, and therefore by the dimensions of extruded filament threads. 3D-printed channel structures might be employed for cell or tissue culture, though a glass slide needs to be incorporated in order to allow microscopic examination of the cells. Most of the materials that are used in FDM 3D printing are also biocompatible, which makes this method an excellent choice for development of devices for cell-based applications.

3.4.3.4) Patterning for paper microfluidics

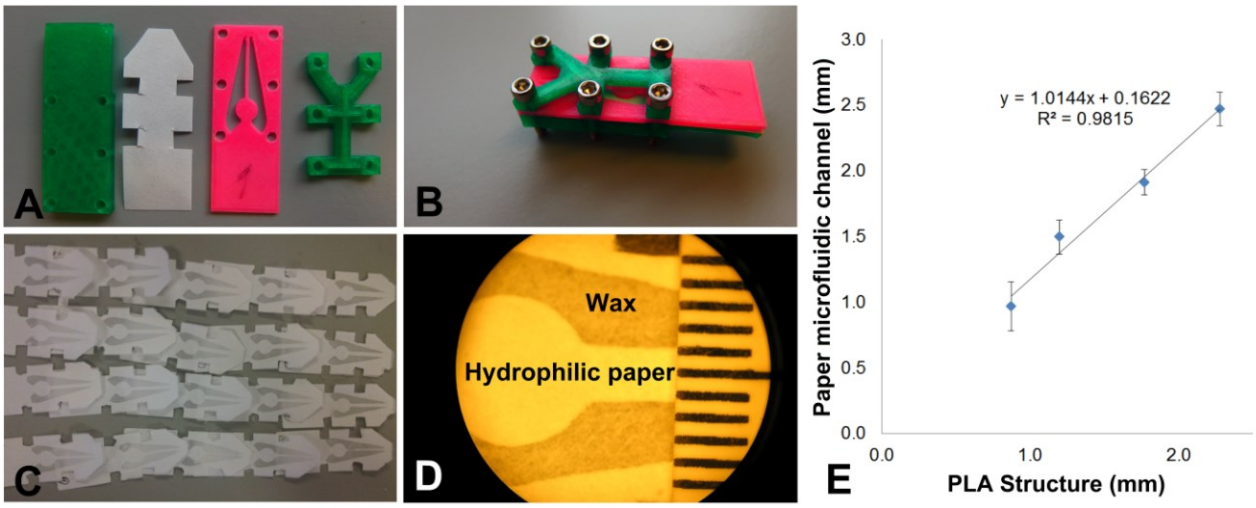

Figure 3.6: Wax patterning approach that used 3D-printed masks to shield the paper from modification. (A) 3D-printed PLA parts (green and pink) and a strip of paper (white). (B) Assembly of the parts with the paper strip sandwiched between the green rectangular base and pink mask. (C) Resulting wax patterns on paper. (D) Microscopic image of a wax pattern defining a paper channel (approximately 2 mm wide), with a ruler for size calibration. (E) Correlation between size of the 3D-printed masks and the actual channel size. Error bars show standard deviations (n=5 per data point).

3D-printed parts can be used in the production of paper microfluidic structures, as we have reported for the patterning of alkyl ketene dimer-treated paper strips[14]. We have also employed FDM to make a tool for wax patterning, as shown in Figure 3.6. The 3D-printed parts (Figure 3.6A-B) successfully shielded parts of the paper from the deposition of molten wax when the assembly in Figure 3.6B was dipped in it. This reproducibly led to clearly defined hydrophilic (untreated paper, white) and hydrophobic (wax-treated, gray) regions (Figure 3.6C-D). The paper channels defined between the wax barriers were characterized with respect to their width (Figure 3.6D-E). Correlation was found between the width of the thin PLA strip of the mask and the size of the resulting paper microfluidic channel. 3D printing is very suitable for the realization of rapid prototyping of different paper microfluidic structures. However, for mass production of paper microfluidic devices, other production methods are more time-efficient.

3.4.3.5) Customizing lab equipment and 3D-printed tools

A last example of the applicability of (FDM) 3D printing for a research lab involves the production of labware, lab tools, or the customization of an experimental setup, which saves money, time and allows for robust and user-friendly experimental setups. Figure 3.7 shows a few such applications in our laboratory.

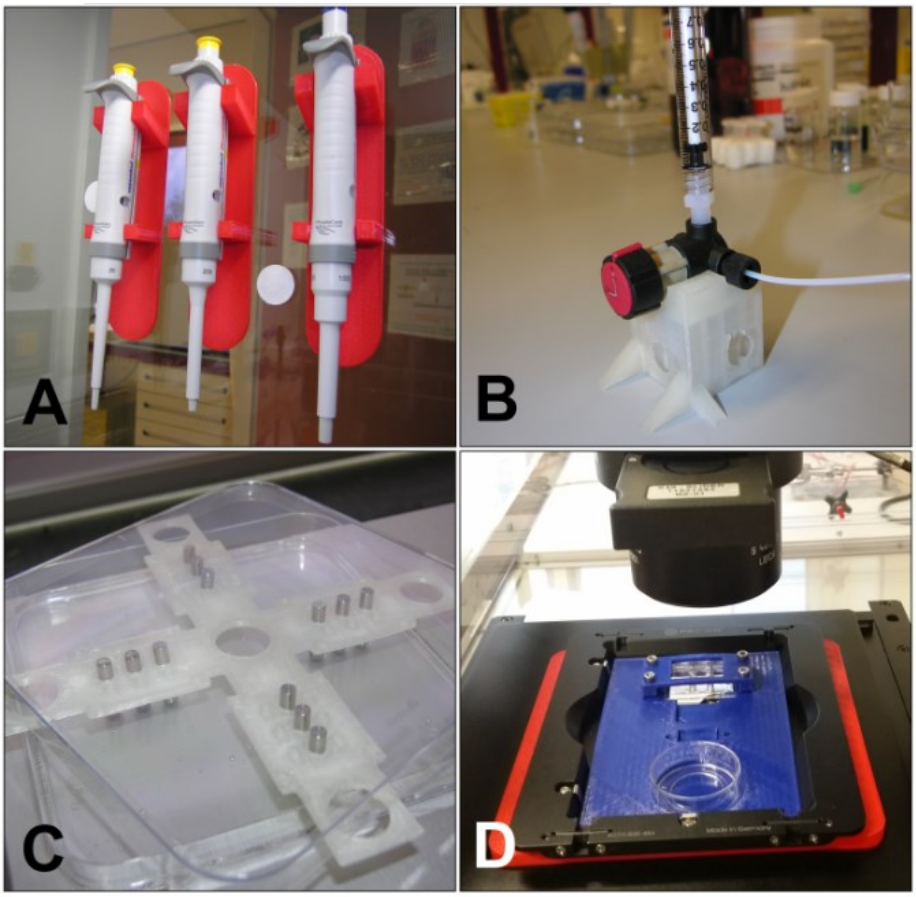

Figure 3.7: Examples of 3D-printed tools, used in a research laboratory. (A) 3D-printed pipet holders (red). (B) A 3D-printed stand for a bulky 4-way valve (colorless). (C) A 3D-printed alignment plate for pins, to create aligned holes when casting a slab of PDMS (colorless). (D) A customized 3D-printed microscope stage for cell cultivation microchips (blue).

3.5) Conclusion

In November 2012 we bought a Felix v.1.5 printer for roughly 1.000 €. At that time we had no real expectations of this technology, and it seemed like an interesting and relatively inexpensive experiment. 3D printing was a new concept in the field of lab-on-a-chip and microfluidics and few labs had experience with this technology. Now, only about 4 years later, we have seen a rapid increase in the number of publications in microfluidics and related fields utilizing this technology. Furthermore, it is now difficult to imagine life in our own lab without 3D printing.

3D printing is a technique that belongs to everybody. The advent of affordable printers has meant the rapid establishment of this technology in many aspects of life besides research. The societal impact of the technology has been growing, meaning that further leaps in the development of this tool are likely in the near future. One big advantage of the common appeal of the 3D printer, is the fact that there is a large interactive community revolving around this topic. This community has proven to be valuable for the research described in this work, as solutions for some of the described problems (as well as some ideas) were developed after consulting various internet forums, such as the RepRap forums and various forums linked to commercially available printers (*e.g.* Felix and Ultimaker). Unfortunately, such information is diffuse and almost impossible to trace to the original authors or inventors, and so their sources do not appear in the list of references for this work.

In relation to other printing approaches, FDM is probably the most accessible. Both the materials and the printer itself are inexpensive. Other advantages of the FDM method include the ease with which different materials can be switched during a print, and the possibility to integrate and embed external components into a single part. Other benefits are the biocompatibility of most FDM materials with tissue and cells, and the wide range of materials available for printing. Drawbacks are mainly related to the resolution and surface smoothness (which is slightly better with other 3D printing approaches, like DLP). However, given the rate of current developments, we expect that (FDM) printers capable of achieving higher resolution will become readily available in the foreseeable future.

It is our hope that this work, as well as all the work cited, will help to convince researchers in the field of microfluidics and lab-on-a-chip that 3D printing indeed offers grand opportunities to do better, more efficient science. This is certainly a technology that can make our jobs as scientists easier, and moreover, stimulate our creativity.

SUPPLEMENTARY INFORMATION

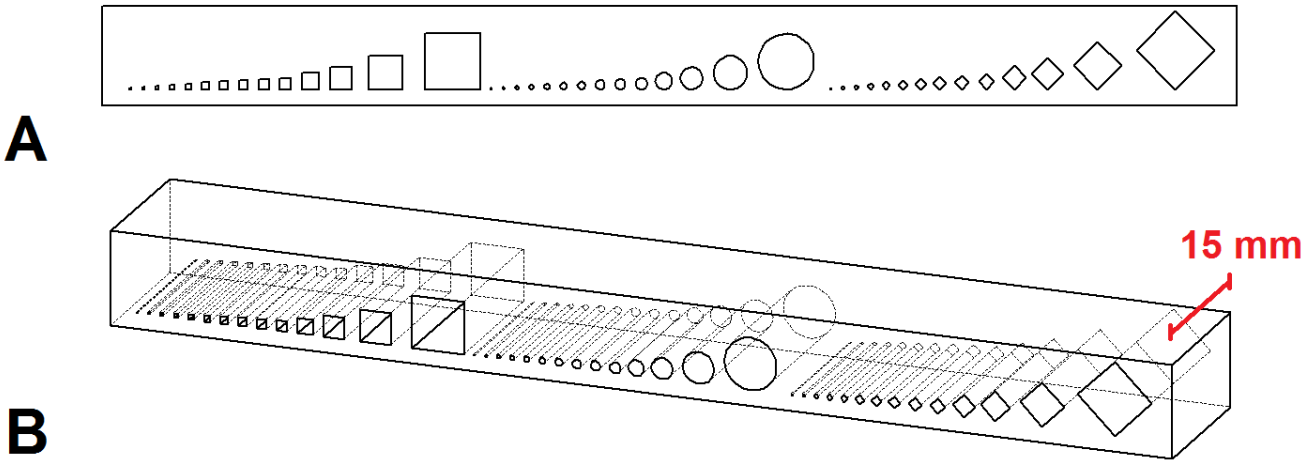

Figure S3.1: SolidWorks model to characterize printing resolution and assess the impact of overhanging structures such as channel ceilings in different designs. The structure shown in the SolidWorks drawings contains embedded channels having rectangular, circular, or diamond-shaped cross-sections of varying sizes. (A) Front view of the structure with embedded channels. (B) 3D view of the same structure as in (A). Three different cross-sectional channel shapes were tested (square, circular and diamond-shaped). The diameter (circular) or diagonal width (square, diamond-shaped) was varied (from left to right, in mm: 0.1, 0.2, 0.3, 0.4, 0.5, 0.6, 0.7, 0.8, 0.9, 1.0, 1.5, 2.0, 3.0, 5.0), while the aspect ratio was kept constant at 1 (channel height = channel width).

Table S3.1: Slice and print information for various 3D-printed test structures and devices

Process	Parameter	Structure for resolution test and PDMS replication molding	Device for leakage prevention test	Device for transparency test
Slicing	*Resolution*	0.13 mm (z) 0.26 mm (xy)	0.13 mm (z) 0.26 mm (xy)	0.13 mm (z) 0.26 mm (xy)
	Infill solidity[a]	1	0.2, 0.5, 1.0	1
	Infill pattern	n/a	Line	n/a
	Shell nr.[b]	1	1, 2, 3, 4	2
Printing	*Printing speed (perimeter / infill)*	25 mm/s; 40 mm/s	25 mm/s; 40 mm/s	25 mm/s; 40 mm/s
	Extruder temp.	200 ^{O}C	200 ^{O}C	200 ^{O}C
	Print bed temp.	60 ^{O}C	60 ^{O}C	60 ^{O}C
	Filament type	PLA EasyFil, red	Transparent PLA	Transparent PLA
Miscellaneous		n/a	n/a	Insert glass slide during the print

[a] Ratio between filament and air in the interior of the part. A low Infill solidity value (e.g. 0.2) leads to a relatively open infill, whereas a high value (e.g. 1) leads to a solid part. See also Fig. S3.2.
[b] Number of adjacent threads of filament that outline all structures.

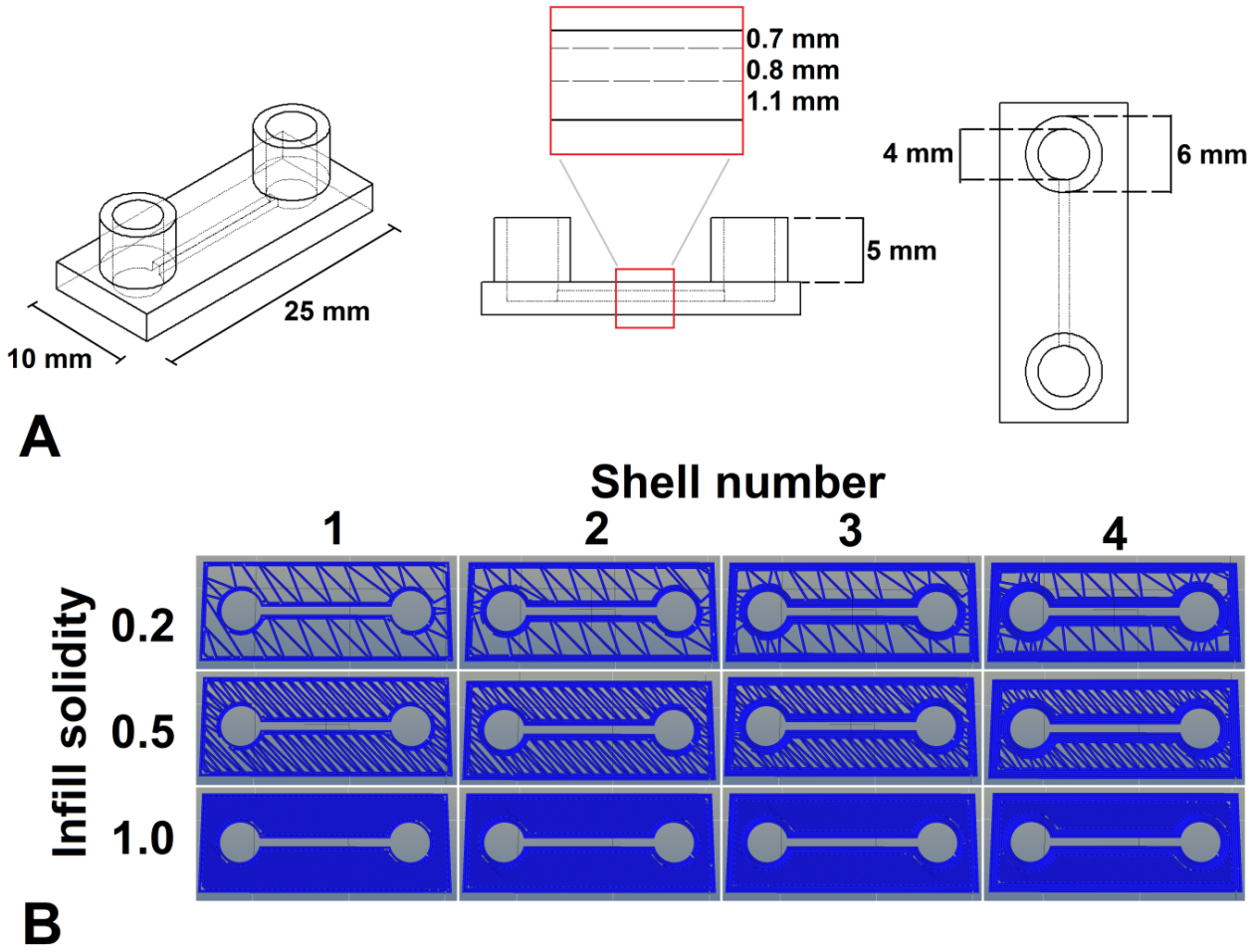

Figure S3.2: (A) SolidWorks design for a device to test prevention of leakage in 3D-printed channels. The embedded channel has a length of 15 mm, width of 0.8 mm and depth of 0.8 mm. The thickness of the PLA channel ceiling is 0.7 mm, whereas the channel base is 1.1 mm thick. (B) Different infill solidities and shell numbers were set in the slicing software to assess their impact on the prevention of leakage.

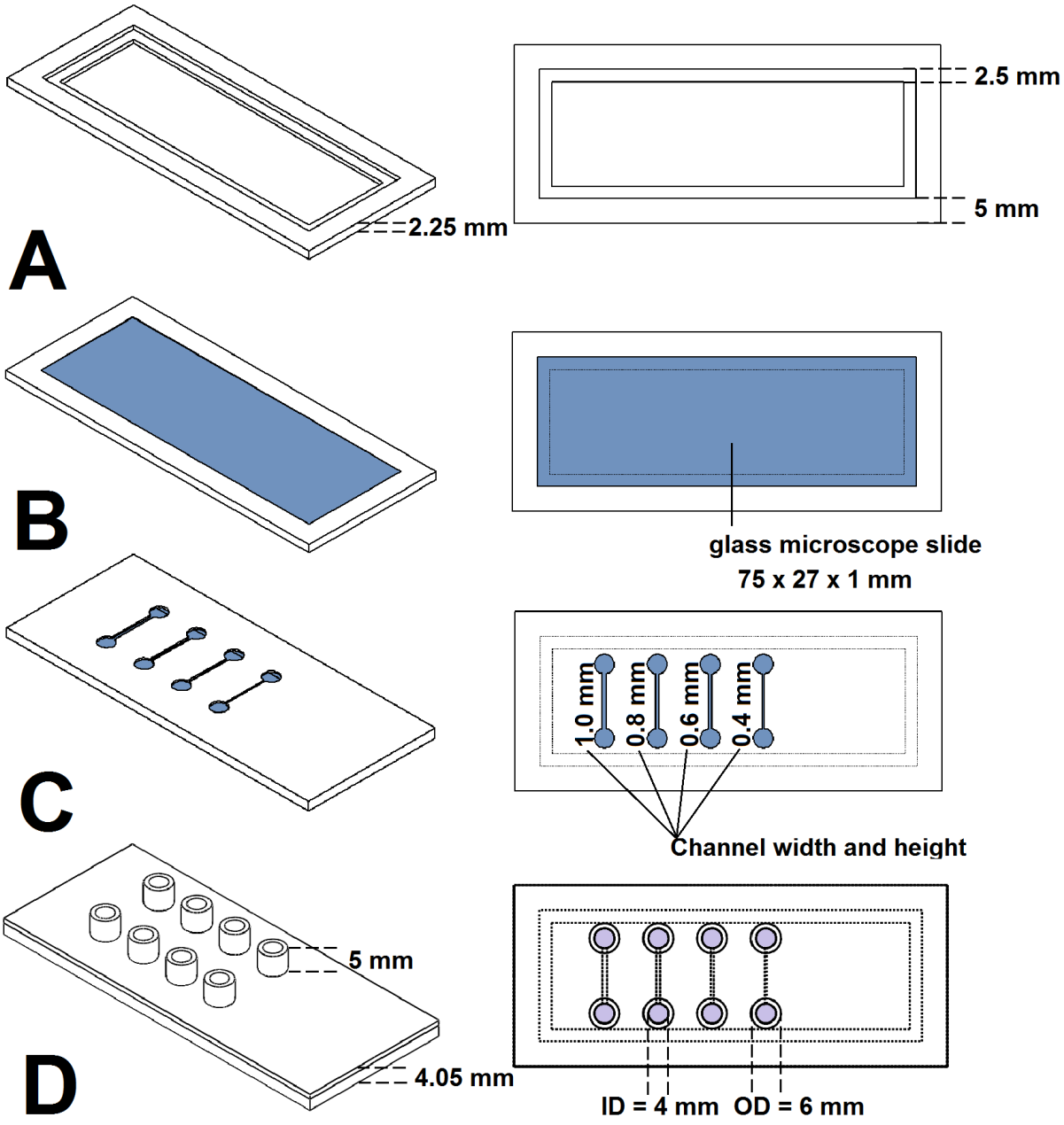

Figure S3.3: Hybrid PLA/glass device to test transparency. A hollow frame was designed in SolidWorks, with an internal cavity the size of a microscope glass slide (27 mm by 75 mm by 1 mm). The device was printed in Transparent PLA. (A) The device was printed up to the point where the cavity walls were completed. (B) The print was then paused and the glass slide (blue) was inserted into the cavity, to form the bottom exterior surface of the device. (C) The print was then continued and PLA channels were printed onto the glass slide, which served as the bottom of the channels. (D) The rectangular channels were sealed by printing transparent PLA over them, and solvent reservoirs were printed on the inlets and outlets of the channels.

Table S3.2: List of tested FDM materials and printing parameters.

Material	Chemical composition	Filament Supplier	Extruder temp. (°C)	Bed temp. (°C)	Rel. print speed[a] (mm/s)	Extruder fan	Brim[b]
PLA Gold (EasyFil)	Polylactic acid	FormFutura	200	60	100%	On	No
Transparent PLA (Premium)	Polylactic acid	FormFutura	200	60	100%	On	No
PLA Soft	Polylactic acid	Orbi-Tech	210	60	50%	On	No
PLA 45	Polylactic acid	Orbi-Tech	170	55	100%	On	No
ABS Orange	Acrylnitrile butadiene styrene	Kunststofshop	225	80	100%	Off	Yes
PC	Polycarbonate	Orbi-Tech	250	80	100%	Off	Yes
PS	Polystyrene	FormFutura	215	80	100%	On	Yes
PVA	Poly vinyl alcohol	Orbi-Tech	185	55	100%	On	No
PET	Polyethylene terephthalate	FormFutura	210	65	100%	On	No
T-Glase	Polyethylene terephthalate	Taulman 3D	210	65	100%	On	No
Arnitel Eco	Thermoplastic Co-Polyester	Formfutura (DSM)	210	60	60%	On	No
Bendlay	Acrylnitrile butadiene styrene	Orbi-Tech	210	65	100%	On	No

[a] Print speed can be predefined in the slicing software. During the print, this speed is regarded as the '100%' value. Print speeds can be adjusted to values between 25% and 300% of the predefined value during the print. In general, for the structures that were printed to test material properties, a basic print speed of 70 mm/s for the infill and 40 mm/s for the perimeter shells was used.

[b] A number of additional shells is printed around the first layer, in order to increase the surface of this layer and thus improve the attachment to the plate. Furthermore, the use of a brim can reduce warping effects.

Protocol S3.1: FDM materials: Solvent compatibility test

Fifteen test structures (2D generic human figures, approximately 14 mm high, 5 mm wide in the torso, with 1 mm wide arms) were printed in each of the 12 FDM materials of interest, 3 for each solvent tested. Each preweighed test structure was put into an individual, preweighed, labeled Eppendorf tube (*exposure tube*). One mL of the solvent to be tested was added to each of three exposure tubes to initiate exposure. Three exposure times were tested, namely 1 hour, 24 hours (1 day) and 168 hours (7 days). During exposure, the tubes were placed on a PS-3D shaker at approximately 40 rpm (Grant Instruments, Cambridgeshire, UK). After the set exposure time had passed, 0.5 mL of the solvent was removed from the tube and placed into a labelled, preweighed Eppendorf tube (*evaporation tube*). The evaporation tube was not sealed, so as to allow the solvent to evaporate in a fume hood. The polymer figure was photographed immediately after the end of exposure. The remaining solvent in the exposure tube was then removed, and the model was allowed to dry in this tube for at least a day. Afterwards, the weight of the material in the evaporation tube was determined as an indication of the amount of material that had dissolved into the solvent. The weight of the dried figure after exposure was also determined. Polymer solvent compatibility was classified based on the following rules:

Table S3.3: Classification of solvent compatibility

Rule (in order of priority)	**Classification**
Dissolved material > 10% of initial mass	--
> 10 % deviation from initial mass in remaining material	--
Loss of structural integrity	--
Dissolved material > 5 % of initial mass	-
> 5 % deviation from initial mass in remaining material	-
Obvious swelling or change in color	-
Dissolved material > 2.5 % of initial mass	+/-
> 2.5 % deviation from initial mass in remaining material	+/-
Dissolved material < 2.5 % of initial mass	+
< 2.5 % deviation from initial mass in remaining material	+

Protocol S3.2: Biocompatibility tests

Cell model: Human Umbilical Vein Endothelial Cells (HUVEC) (Lonza, CC-2519, pooled donors, Benelux B.V., Breda, The Netherlands) were cultured to confluency in T25 flasks for 2 to 4 passages before being seeded in 12-well plates. HUVEC were harvested from T25 bottles by trypsinization (0.05% trypsin solution in sterile PBS; 20 µL/cm^2 of trypsin solution), counted and resuspended in fresh endothelial cell (EC) medium at a concentration of 4500 cells/µL. Afterwards they were kept on ice until further use. The Eppendorf tube containing the cells was gently shaken to resuspend the cells just before seeding 5 µL in 12-well plates, which had been coated with a 1% solution of gelatin (porcine skin, Sigma Aldrich, Steinheim, Germany) according to the supplier's protocol.

Cell cultivation conditions: Endothelial cell medium (EC medium) consisted of RPMI 1640 (Lonza Benelux B.V., Breda, The Netherlands); endothelial cell growth factor (50 µg/mL isolated from bovine brain); L-glutamine (2 mM; Gibco-BRL, Paisley, Scotland); heparin (5 U; Leo Pharm. Prod., Weesp, The Netherlands); K-penicillin G (100 IE/mL; Astellas Pharma Europe B.V., Leiderdorp, The Netherlands); streptomycin (100 µg/mL; Fisiopharm, Italy); and fetal calf serum (20% v/v; Hyclone, Perbio Science, Etten-Leur, The Netherlands). The medium did not contain the pH indicator, phenol red. For the exposure experiments, HUVEC were incubated (Esco Cell Culture CO_2 Incubator) in 12-well plates at 37°C, with 95% air and 5% CO_2. Polymer exposure/biocompatibility tests were started when HUVEC cultures had achieved 60-80% confluency, which was generally the case after an overnight cultivation. Fresh medium was added at the start of the experiment and was not refreshed for the duration of the experiment (18h).

Tissue model: Preparation of PCLS was done based on the protocol by De Graaf et al.[27] Under isofluorane/O_2 anesthesia, the livers from male Wistar rats (300 g, free access to food and water; Charles River, Sulzfeld, Germany) were excised and placed in ice-cold University of Wisconsin (UW) solution (DuPont Critical Care, Waukegab, IL). Cores (5 mm in diameter) were cut from the livers. A Krumdieck slicer (Alabama R&D, Munford, AL) was used for slicing the cores into precision-cut liver slices which were approximately 200 µm thick, 5 mm in diameter, and had a wet weight of 5 mg. Slices were collected in ice-cold Krebs–Henseleit buffer with 25 mM d-glucose (Merck, Darmstadt, Germany), 25 mM $NaHCO_3$ (Merck), and 10 mM HEPES (MP Biomedicals, Aurora, OH) added, and saturated with 95% O_2 and 5% CO_2. PCLS were then transferred to be stored up to 4 hours in ice-cold UW solution until incubation was started.

Tissue cultivation conditions: Williams Medium E with L-glutamine (Invitrogen, Paisly, Scotland) (WME), supplemented with 50 mg/mL gentamycin and 25 mM glucose (Invitrogen), was used for incubation. Aliquots of 1.3 mL of WME were added to the wells of a 12-well culture plate. The plates were then equilibrated in a Panasonic (Osaka, Japan) shaking incubator (90 rpm) at 37°C, in which the gas composition was continuously kept at

80% O_2 and 5% CO_2. After the medium had reached 37°C, a slice was inserted in each well, after which the plates were placed in the shaking incubator for 1 hour (pre-incubation). This pre-incubation allowed for the removal of cell debris left over after slicing, and the restoration of PCLS function after the slicing procedure. After pre-incubation, control slices were taken for both the LDH and ATP assays. The remaining slices were transferred after pre-incubation to new wells for the 24-h polymer exposure tests, as described in Section 3.3.2.3 of the main text.

MTT test (HUVEC): This assay measures to what extent NAD(P)H-dependent cellular oxidoreductase enzymes reduce the tetrazolium dye 3-(4,5-dimethylthiazol-2-yl)-2,5-diphenyltetrazolium bromide (MTT) to the insoluble compound, formazan. Formazan has a purple color that can be measured by absorbance with a spectrophotometer. The more intense the purple color, the more metabolically active (and viable) the cells.

MTT and sodium dodecyl sulfate (SDS) for the material toxicity study were purchased (Thermo Fisher Scientific Inc.) in the form of the MTT Cell Proliferation Assay Kit. After 18h of incubation, the 3D-printed rings were removed from the wells and EC medium was replaced by EC medium with MTT (10 µL of 12 mM MTT in 100 µL EC medium). The cells were then incubated for 2 hours. After the reaction, 100 µL of a 0.01 M solution of HCl containing 100 g/L SDS was added to each well and mixed. The well plates were then incubated for 4 hours at 37°C. Afterwards, the absorbance of the samples was measured at 570 nm with a ThermoMax Microplate reader (Molecular Devices, Sunnyvale, CA). Positive controls were included in every experiment. For the positive control, HUVEC were cultured in the absence of the 3D-printed material, alongside HUVEC exposed to 3D-printed rings. Negative controls in the experiment were performed in wells without HUVEC and filled only with EC medium, kept under the same conditions and for the same time as HUVEC exposed to 3D-printed rings.

LDH leakage assay (PCLS): LDH leakage into the medium was used as an indicator of cell membrane integrity. After 1h of pre-incubation, 3 control slices were each collected in 1.3 mL of fresh WME. After 24 hours, 200-µL samples of medium were taken from all wells. Samples were stored at 4°C for no longer than 24 hours until measurement, to avoid degradation of the LDH. Control slices were homogenized using a bead beater (45 s, Biospec Products, Bartlesville, OK) and centrifuged (16,100 g; 2.5 minutes), after which the supernatant was used for the assay. LDH was measured using the CytoTox-ONE Homogenous Membrane Integrity assay kit (Promega, Madison, WI). Fifty µL of sample was mixed with an equal amount of the substrate mix at room temperature in a black 96-well plate. After 10 minutes, the reaction was stopped by adding 25 µL of stop solution to each well. Fluorescence intensity was measured at 590 nm after excitation at 560 nm using a Spectramax Gemini XPS fluorescence plate-reader (Molecular Devices, Sunnyvale, CA). LDH baseline was obtained by assessment of the LDH content in PCLS (for every batch separately) not submitted to an experiment, taken after pre-incubation. The LDH leakage of slices for a given

experiment was compared to this baseline LDH content. Positive controls were established by unexposed PCLS incubation for the same time and the same conditions as PCLS exposed to 3D-printed materials.

The possible influence of the 3D-printed materials on the fluorescence intensity in this test was also determined. Samples were taken from the medium in which printed rings were incubated without PCLS for 24 hours, and analyzed using the same protocol described above.

ATP and protein content assay (PCLS): ATP content was used as an indicator of the ability of the slices to synthesize ATP, the most abundant chemical energy-carrier in the cell. After 24 hours of incubation, slices were collected, transferred to 1 mL of 2 mM EDTA in 70% ethanol (pH 10.9), immediately frozen in liquid nitrogen and stored at -80°C until measurement. For analysis, the slices were thawed on ice and then homogenized using a bead beater (45 s, Biospec Products, Bartlesville, OK) and centrifuged (16,100 g; 5 minutes; 4°C). The supernatant was taken and diluted 10 times with 0.1 M Tris HCl buffer (with 2 mM EDTA; pH 7.8). ATP assessment was done in a black 96-well plate using the Bioluminescence Assay Kit CLS II (Roche, Mannheim, Germany) and an ATP calibration line, measured according to the protocol supplied by the manufacturer. Luminescence was measured with a LumiCount plate reader (Packard BioScience, Downers Grove, IL). To normalize for the size of the slices, the protein content of the same slices was determined. For this, the slice homogenate was dried and incubated for 30 minutes at 37°C in 200 µL of 5 M NaOH. Eight hundred µL of ultrapure H_2O was added, after which the samples were homogenized again (45 s) with the bead beater. Protein content was measured with the Bio-Rad DC Protein Assay (Bio-Rad, Munich, Germany), using a calibration line obtained with standard samples of bovine serum albumin. Absorbance was measured at 650 nm with a ThermoMax Microplate Reader (Molecular Devices, Sunnyvale, CA). To account for the varying ATP content of different livers, the normalized ATP content (pmol/µg protein) was expressed as a percentage of the average ATP content of the positive control slices for that experiment. For the positive control, PCLS were incubated in the absence of the 3D-printed material, alongside PCLS exposed to 3D-printed rings. Moreover, during each experiment, three slices were taken and frozen right after pre-incubation to confirm viability of the liver used in that experiment.

Protocol S3.3: PDMS replication and device fabrication

The 3D-printed masters were placed in a vacuum desiccator for 20 minutes with a plastic cup, containing a few drops of hexamethyldisilazane (HMDS, Sigma Aldrich, Steinheim, Germany). This would later facilitate the removal of cured PDMS from the masters, probably by the formation of a thin hydrophobic coating over the printed parts. The part was then thoroughly rinsed with water. Elastomer and curing agent for PDMS (Dow Corning, Auburn, MI) were mixed 10:1 (m/m) and stirred for a few minutes. The mixture was placed in a vacuum desiccator for 30 minutes to remove air bubbles from the liquid polymer mixture, then poured onto the master and allowed to cure overnight at 40°C on a hot plate. After curing, the PDMS was peeled from the master. Inlet and outlet holes were punched into the PDMS with a biopsy puncher (d = 1.5 mm, Kai Medical, Solingen, Germany). The channels were sealed by bonding the PDMS replicate to a flat slab of cured PDMS. This was achieved by first exposing both parts to oxygen plasma for 30s (29.6W, 350 mTorr) in a plasma cleaner (PDC-0002, Harrick Plasma, Ithaca, NY), after which the parts were pressed together. Devices were firmly bonded by the time they were employed, in less than 10 minutes in some cases.

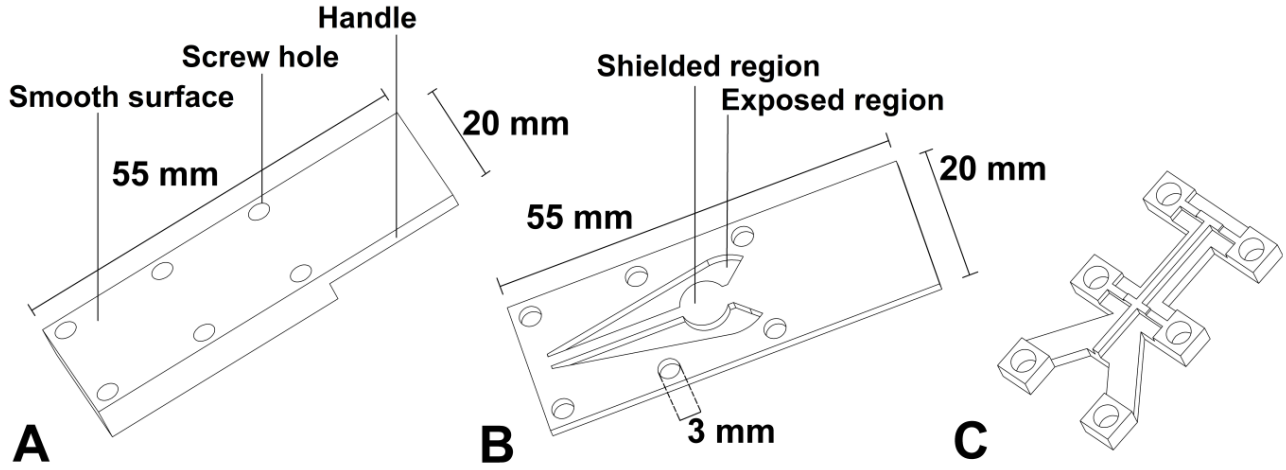

Figure S3.4: SolidWorks drawings for the parts used in the 3D-printed tool made for patterning paper analytical devices with the wax-dipping approach. (A) The flat base with screw holes on to which the paper to be patterned is placed; (B) this drawing shows the 3D-printed mask with openings through which molten wax can contact the paper, making it hydrophobic; (C) structure with screw holes to apply additional pressure on the mask in the center.

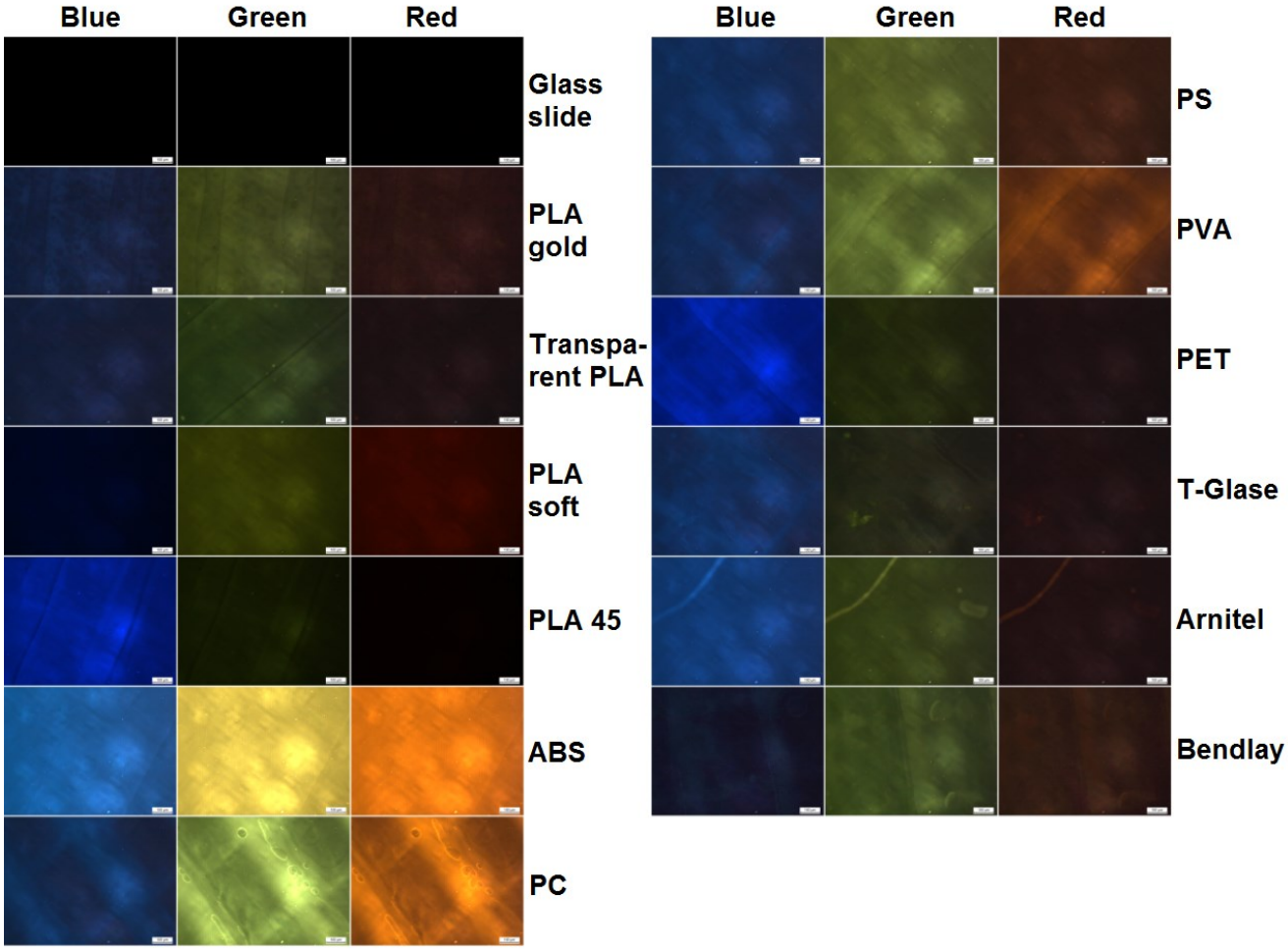

Figure S3.5: Autofluorescence of the twelve FDM materials in the blue (ex/em 430-445/460-500 nm), green (ex/em 450-488/505-545 nm) and red (ex/em 530-557/575-647 nm) range, as compared to glass (black images, top left).

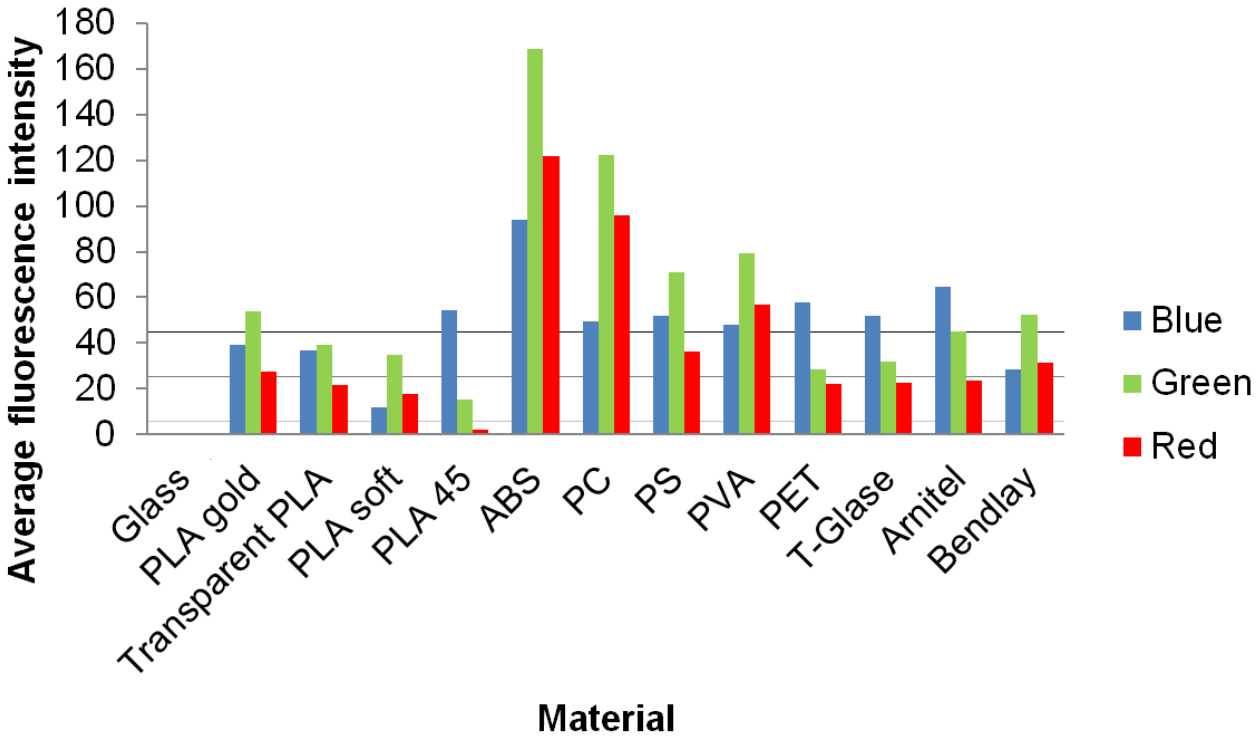

Figure S3.6: Numerical data for the autofluorescence test. The average color intensity (i.e. the average of the intensities for the red, green and blue components of the RGB model) of the photographs in Figure S3.5 was measured with ImageJ (max. value is 255, which represents a white pixel). Autofluorescence was considered negligible (-) if the value remained below 5, acceptable (+/-) between 5 and 25, strong (+) between 25 and 45 and very strong (++) above 45. These thresholds are indicated by the straight horizontal lines in the graph.

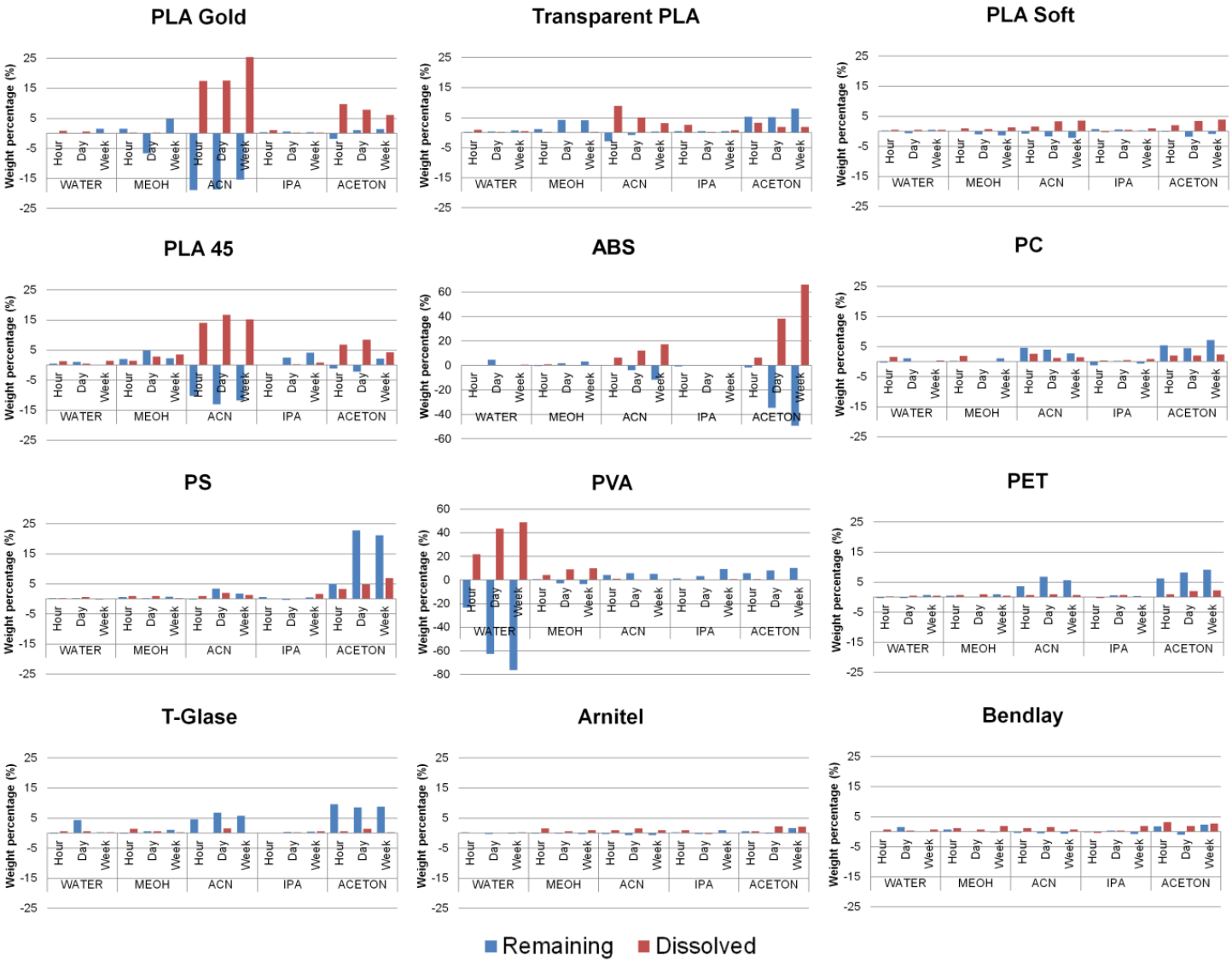

Figure S3.7: Solvent compatibility study for 12 FDM filaments. 3D-printed figures were exposed to five different solvents (water, methanol (MeOH), acetonitrile (ACN), isopropanol (IPA), and acetone) for (i) an hour, (ii) a day (24h), or (iii) a week (168h) as described in Protocol S3.1. The amount of material which had dissolved into the solvent was determined by weighing the residue in the evaporation tube after complete evaporation (red). Similarly, the change in the amount of material making up the initial structure was determined by weighing the dry structure in the exposure tube (blue). These amounts were all related to the original weight of each figure.

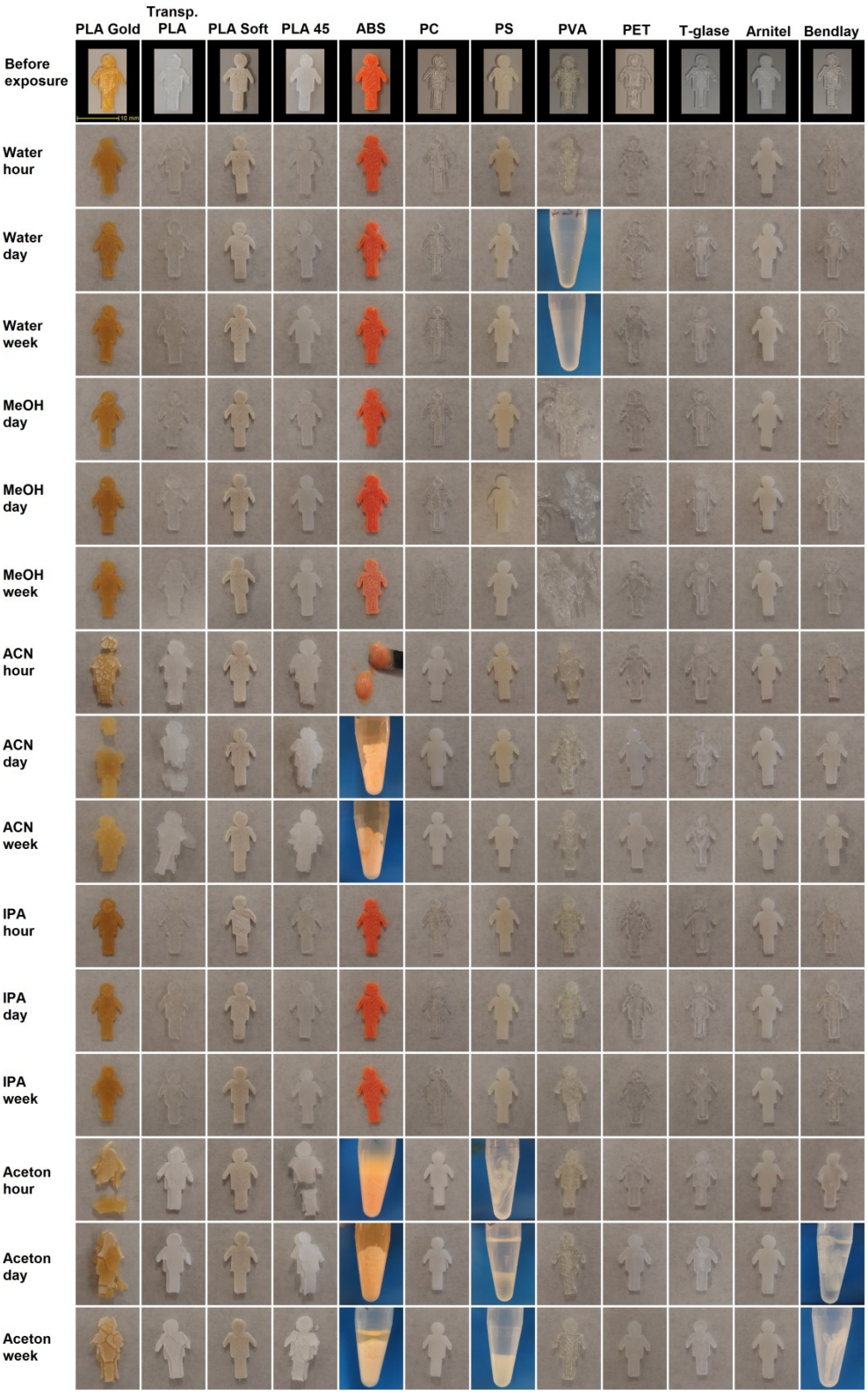

Figure S3.8: Photographs of 3D-printed figures after exposure to different solvents for an hour, a day (24h) or a week (168h). In some cases, loss of integrity of the figures was rapid and/or extreme.

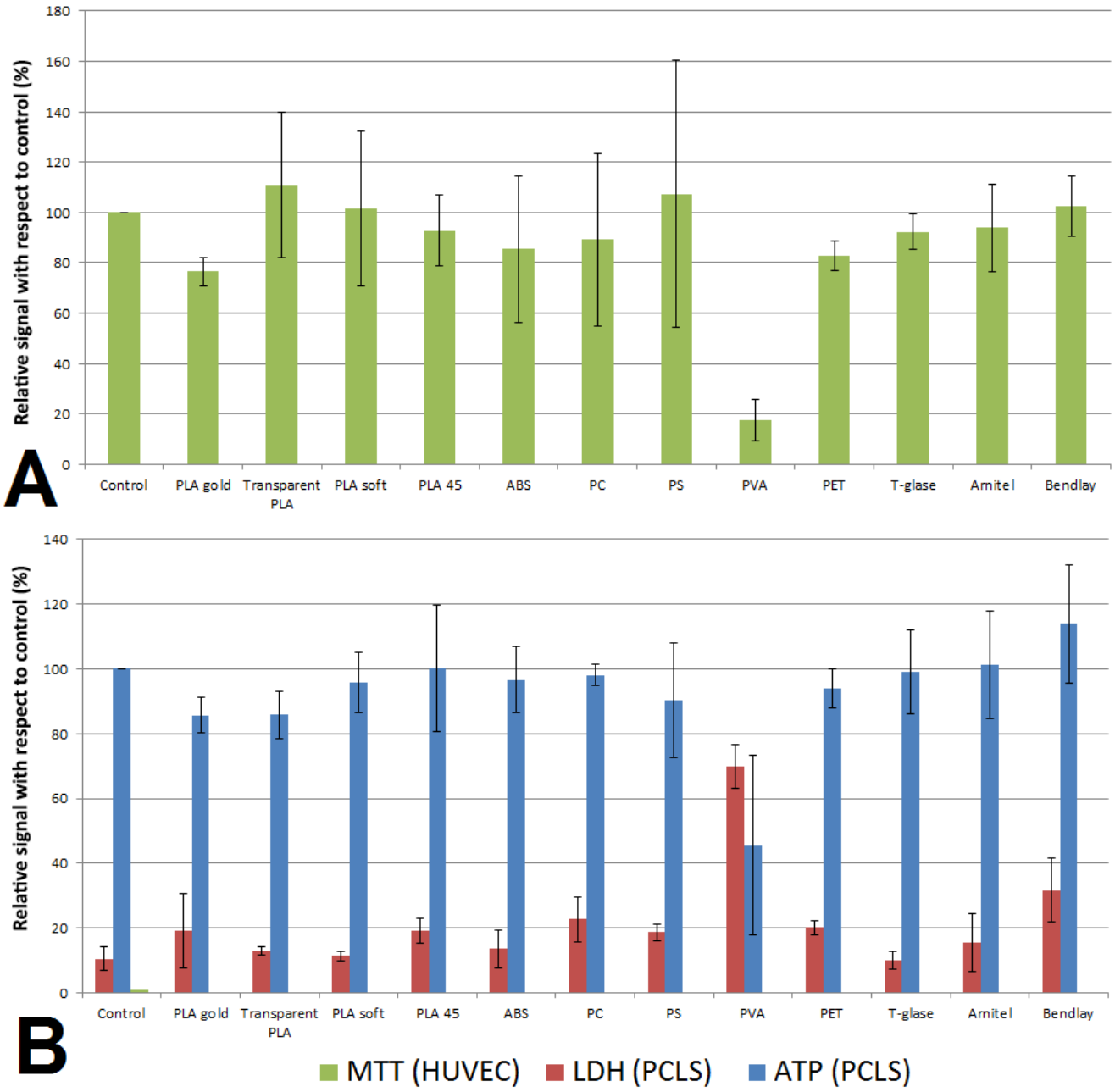

Figure S3.9: Biocompatibility of the FDM materials. (A) Absorbance values for HUVEC incubated for 18h with different 3D-printed materials relative to the positive control. All 3D-printed materials show biocompatibility with HUVEC cultures except PVA ($p=0.009$). This data was collected in three independent experiments (3 cell batches), each performed in triplicate for every material. Large standard deviations are caused by the different numbers of cells in the confluent HUVEC layers. This cell type will modify its size and shape in order to create space for proliferated cells, which resulted in different observed cell densities in the experiments. Furthermore, proliferation rates of HUVEC from the same source might vary because of the cell passage number. In our experiments, we used HUVEC from passage 3 (two experiments) and 4 (one experiment), which is generally accepted in experiments with these cells. They are known to retain their *in vivo* phenotype *in vitro* during early passages. (B) LDH leakage is expressed as a percentage of the average LDH content of control slices measured after the pre-incubation step. Most LDH leakage into the medium occurs during this pre-incubation (39±25%;

see Figure S3.12), as the slices recover from the slicing procedure and cell debris is removed. After 24 hours of incubation in fresh medium with printed polymer rings, slices incubated with all materials show some leakage of LDH into the medium. However, only the amount of LDH leaked out of slices incubated with a PVA ring differs significantly ($p=2*10^{-7}$) from the control group, where PCLS were incubated for 24 hours with no printed material. ATP content, normalized for the protein content, is expressed as a percentage of the average, normalized ATP content of the control slices (24 hours of incubation with no printed material). The control slices are therefore considered as having a 100% normalized ATP content. After 24 hours of incubation, none of the groups showed a significant deviation from the control group, except PVA ($p=0.002$).

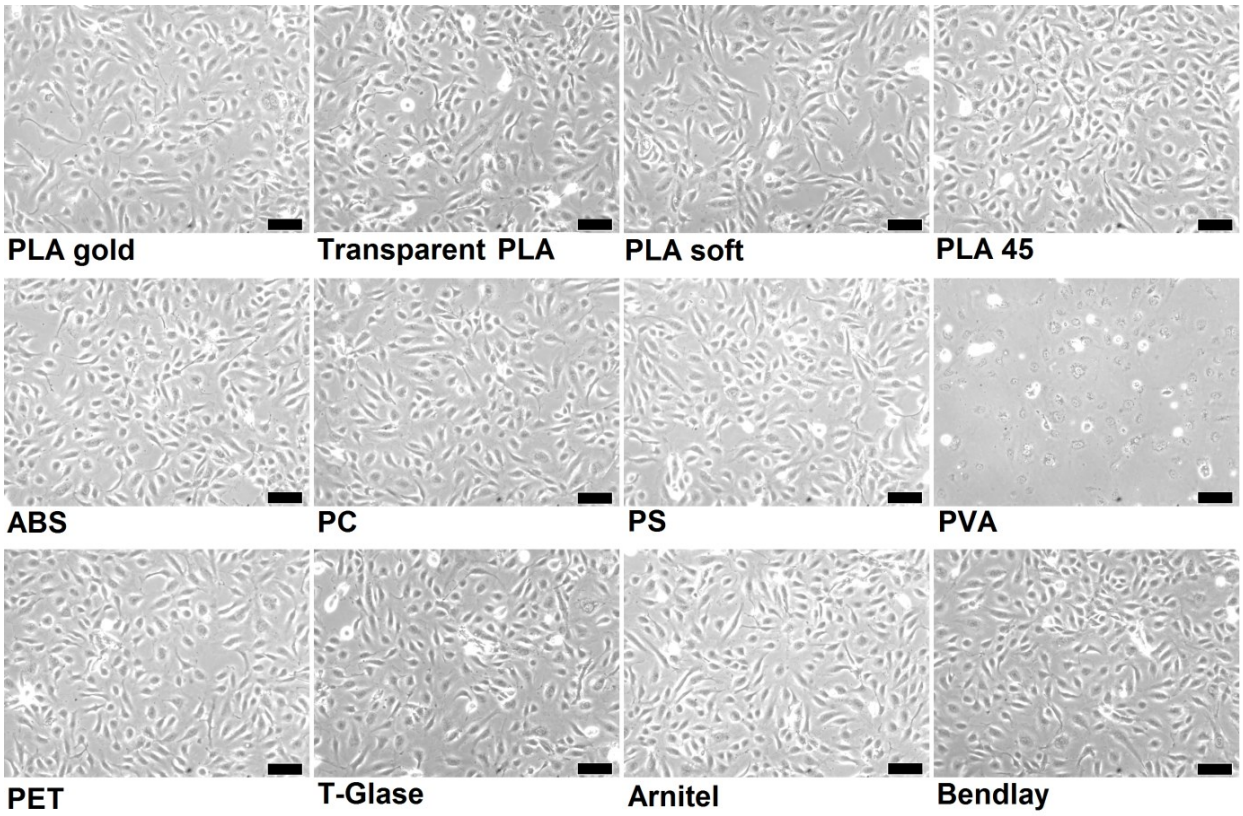

Figure S3.10: Photos of HUVEC cultures acquired after 18h of exposure to 3D-printed materials in 12-well plates. Only PVA shows toxicity towards the HUVEC, as can be concluded by the fact that few HUVEC remain, and those that are still visible are small and misshapen. Magnification of the objective was 10x. The scale bar represents 100 μm (bottom right corner).

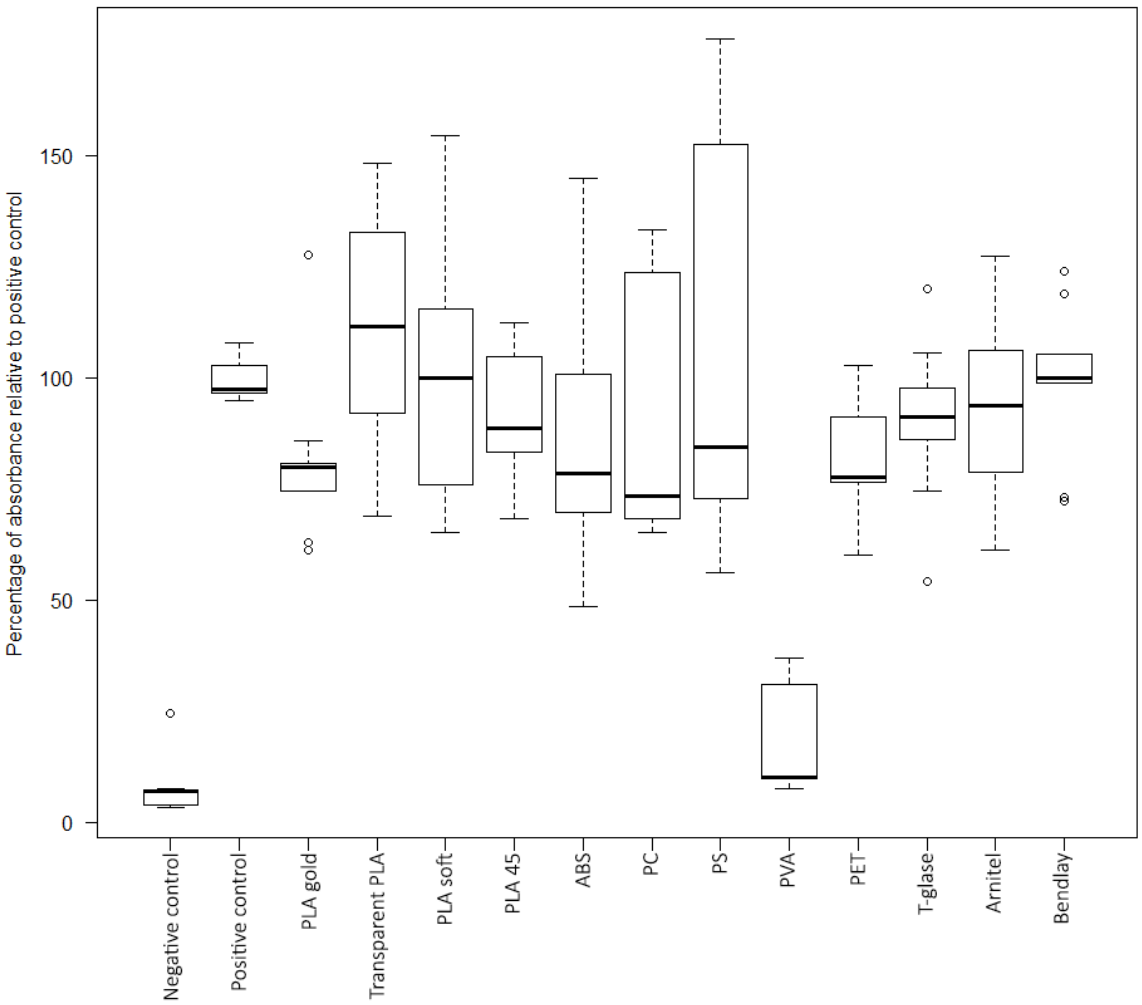

Figure S3.11: Boxplot of the results of the MTT assay on HUVEC cultured with 3D-printed materials. The boxplots were used to visually identify outliers in the data (small circles outside the boxes and whiskers of the plots). These data points were removed prior to calculation of means and standard deviations and performance of ANOVAs.

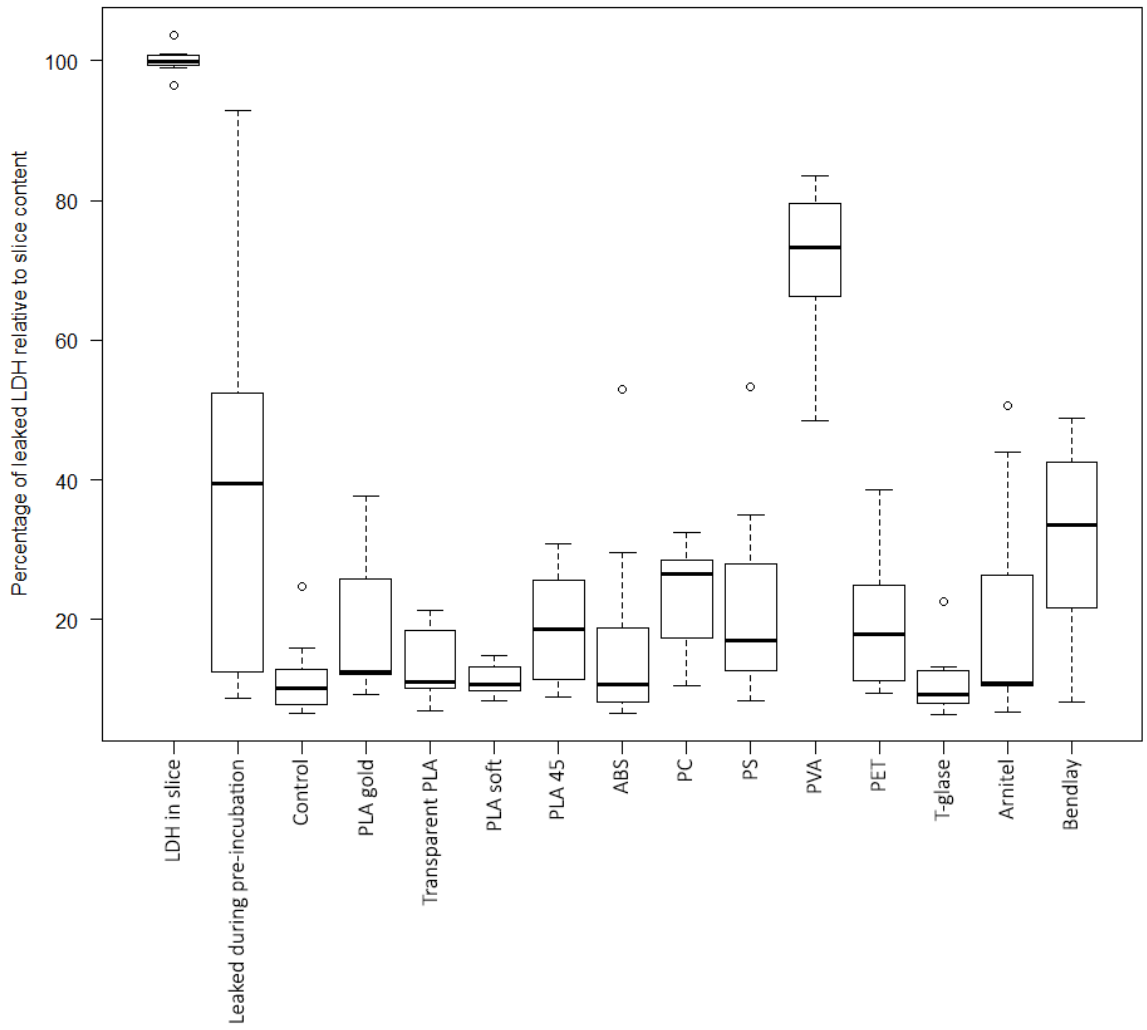

Figure S3.12: Boxplot of the results of the LDH assay on PCLS cultured with various materials. The boxplots were used to visually identify outliers in the data (small circles outside the boxes and whiskers of the plots). These data points were removed prior to calculation of means and standard deviations and performance of ANOVAs. The large variation in LDH content leaked during pre-incubation is as expected[33], as the pre-incubation serves to remove cellular debris resulting from the slicing procedure[34].

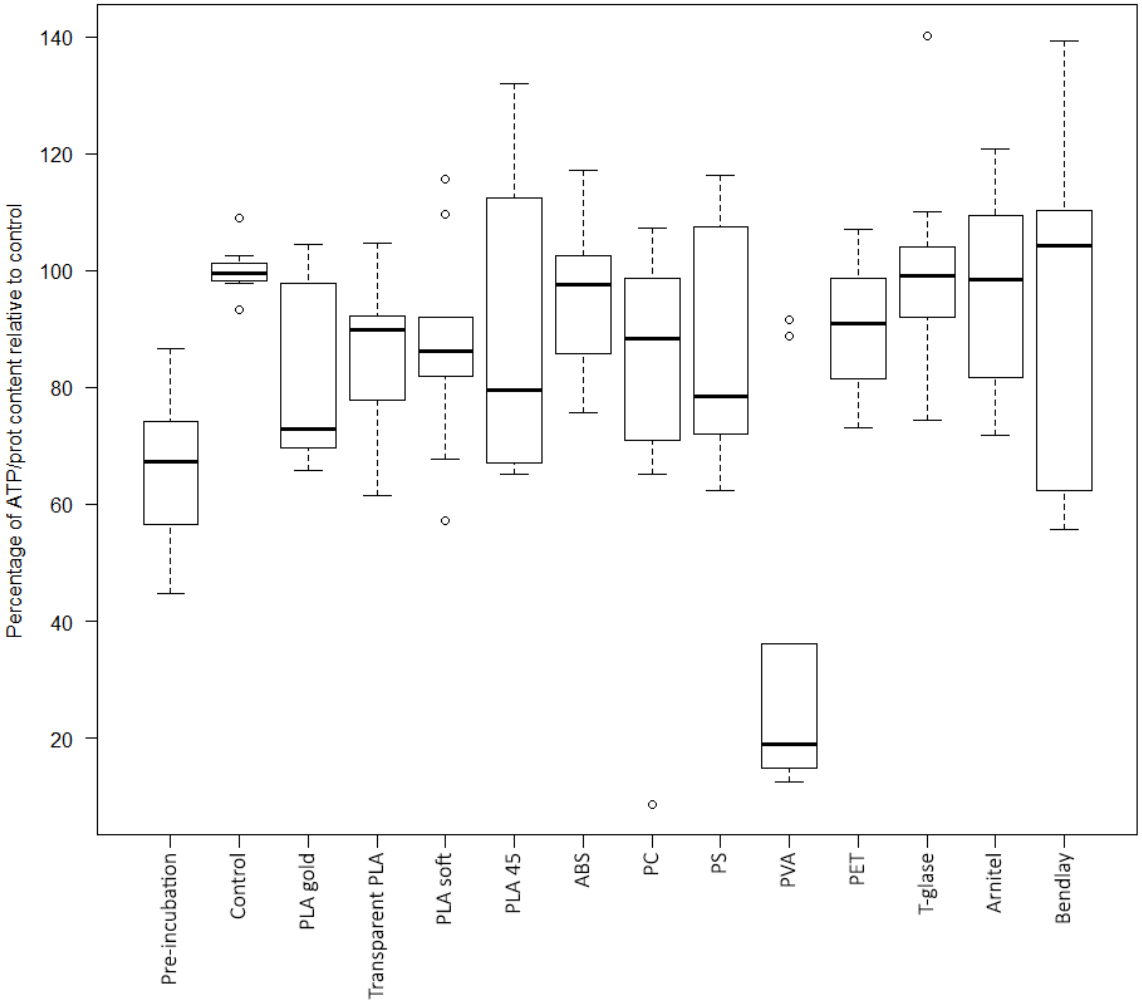

Figure S3.13: Boxplot of the results of the ATP assay on PCLS cultured with various materials (relative to protein content). The boxplots were used to visually identify outliers in the data (small circles outside the boxes and whiskers of the plots). These data points were removed prior to calculation of means and standard deviations and performance of ANOVAs.

References

(1) Gross, B. C.; Erkal, J. L.; Lockwood, S. Y.; Chen, C.; Spence, D. M. Evaluation of 3D Printing and Its Potential Impact on Biotechnology and the Chemical Sciences. *Anal. Chem.* **2014**, *86* (7), 3240–3253.

(2) Ho, C. M. B.; Ng, S. H.; Li, K. H. H.; Yoon, Y.-J. 3D Printed Microfluidics for Biological Applications. *Lab Chip* **2015**, *15* (3), 3627–3637.

(3) Au, A. K.; Huynh, W.; Horowitz, L. F.; Folch, A. 3D-Printed Microfluidics. *Angew. Chemie - Int. Ed.* **2016**, *55* (12), 3862–3881.

(4) Kitson, P. J.; Rosnes, M. H.; Sans, V.; Dragone, V.; Cronin, L. Configurable 3D-Printed Millifluidic and Microfluidic "Lab on a Chip" Reactionware Devices. *Lab Chip* **2012**, *12* (18), 3267–3271.

(5) Anderson, K. B.; Lockwood, S. Y.; Martin, R. S.; Spence, D. M. A 3D Printed Fluidic Device That Enables Integrated Features. *Anal. Chem.* **2013**, *85* (12), 5622–5626.

(6) Shallan, A. I.; Smejkal, P.; Corban, M.; Guijt, R. M.; Breadmore, M. C. Cost-Effective Three-Dimensional Printing of Visibly Transparent Microchips within Minutes. *Anal. Chem.* **2014**, *86* (6), 3124–3130.

(7) Femmer, T.; Jans, A.; Eswein, R.; Anwar, N.; Moeller, M.; Wessling, M.; Kuehne, A. J. C. High-Throughput Generation of Emulsions and Microgels in Parallelized Microfluidic Drop-Makers Prepared by Rapid Prototyping. *ACS Appl. Mater. Interfaces* **2015**, *7*, 12635–12638.

(8) Krejcova, L.; Nejdl, L.; Rodrigo, M. A. M.; Zurek, M.; Matousek, M.; Hynek, D.; Zitka, O.; Kopel, P.; Adam, V.; Kizek, R. 3D Printed Chip for Electrochemical Detection of Influenza Virus Labeled with CdS Quantum Dots. *Biosens. Bioelectron.* **2014**, *54*, 421–427.

(9) Salentijn, G. IJ.; Permentier, H. P.; Verpoorte, E. 3D-Printed Paper Spray Ionization Cartridge with Fast Wetting and Continuous Solvent Supply Features. *Anal. Chem.* **2014**, *86*, 11657–11665.

(10) Comina, G.; Suska, A.; Filippini, D. PDMS Lab-on-a-Chip Fabrication Using 3D Printed Templates. *Lab Chip* **2014**, *14* (2), 424–430.

(11) Chan, H. N.; Chen, Y.; Shu, Y.; Chen, Y.; Tian, Q.; Wu, H. Direct, One-Step Molding of 3D-Printed Structures for Convenient Fabrication of Truly 3D PDMS Microfluidic Chips. *Microfluid. Nanofluidics* **2015**, *19*, 9–18.

(12) Hwang, Y.; Paydar, O. H.; Candler, R. N. 3D Printed Molds for Non-Planar PDMS Microfluidic Channels. *Sensors Actuators A Phys.* **2015**, *226*, 137–142.

(13) Bonyár, A.; Sántha, H.; Varga, M.; Ring, B.; Vitéz, A.; Harsányi, G. Characterization of Rapid PDMS Casting Technique Utilizing Molding Forms Fabricated by 3D Rapid Prototyping Technology (RPT). *Int. J. Mater. Form.* **2014**, *7* (2), 189–196.

(14) Salentijn, G. IJ.; Hamidon, N. N.; Verpoorte, E. Solvent-Dependent On/Off Valving Using Selectively Permeable Barriers in Paper Microfluidics. *Lab Chip* **2016**, *16*, 1013–1021.

(15) Hyde, J.; MacNicol, M.; Odle, A.; Garcia-Rill, E. The Use of Three-Dimensional Printing to Produce in Vitro Slice Chambers. *J. Neurosci. Methods* **2014**, *238*, 82–87.

(16) Paydar, O. H.; Paredes, C. N.; Hwang, Y.; Paz, J.; Shah, N. B.; Candler, R. N. Characterization of 3D-Printed Microfluidic Chip Interconnects with Integrated O-Rings. *Sensors Actuators A Phys.* **2014**, *205*, 199–203.

(17) Kitson, P. J.; Marshall, R. J.; Long, D.; Forgan, R. S.; Cronin, L. 3D Printed High-Throughput Hydrothermal Reactionware for Discovery, Optimization, and Scale-Up. *Angew. Chemie Int. Ed.* **2014**, *53* (47), 12723–12728.

(18) Lücking, T. H.; Sambale, F.; Schnaars, B.; Bulnes-Abundis, D.; Beutel, S.; Scheper, T. 3D-Printed Individual Labware in Biosciences by Rapid Prototyping: In Vitro Biocompatibility and Applications for Eukaryotic Cell Cultures. *Eng. Life Sci.* **2015**, *15*, 57–64.

(19) Lücking, T. H.; Sambale, F.; Beutel, S.; Scheper, T. 3D-Printed Individual Labware in Biosciences by Rapid Prototyping: A Proof of Principle. *Eng. Life Sci.* **2015**, *15*, 51–56.

(20) Ude, C.; Hentrop, T.; Lindner, P.; Lücking, T. H.; Scheper, T.; Beutel, S. New Perspectives in Shake Flask pH Control Using a 3D-Printed Control Unit Based on pH Online Measurement. *Sensors Actuators B Chem.* **2015**, *221*, 1035–1043.
(21) Tyson, A. L.; Hilton, S. T.; Andreae, L. C. Rapid, Simple and Inexpensive Production of Custom 3D Printed Equipment for Large-Volume Fluorescence Microscopy. *Int. J. Pharm.* **2015**, *494* (2), 651–656.
(22) Wardyn, J. D.; Sanderson, C.; Swan, L. E.; Stagi, M. Low Cost Production of 3D-Printed Devices and Electrostimulation Chambers for the Culture of Primary Neurons. *J. Neurosci. Methods* **2015**, *251*, 17–23.
(23) Zwicker, A. P.; Bloom, J.; Albertson, R.; Gershman, S. The Suitability of 3D Printed Plastic Parts for Laboratory Use. *Am. J. Phys.* **2014**, *83* (3), 281–285.
(24) Takenaga, S.; Schneider, B.; Erbay, E.; Biselli, M.; Schnitzler, T.; Schöning, M. J.; Wagner, T. Fabrication of Biocompatible Lab-on-Chip Devices for Biomedical Applications by Means of a 3D-Printing Process. *Phys. Status Solidi A* **2015**, *212* (6), 1347–1352.
(25) Schneider, C. A.; Rasband, W. S.; Eliceiri, K. W. NIH Image to ImageJ: 25 Years of Image Analysis. *Nat. Methods* **2012**, *9* (7), 671–675.
(26) Bachetti, T.; Morbidelli, L. Endothelial Cells in Culture: A Model for Studying Vascular Functions. *Pharmacol. Res.* **2000**, *42* (1), 9–19.
(27) de Graaf, I. A. M.; Olinga, P.; de Jager, M. H.; Merema, M. T.; de Kanter, R.; van de Kerkhof, E. G.; Groothuis, G. M. M. Preparation and Incubation of Precision-Cut Liver and Intestinal Slices for Application in Drug Metabolism and Toxicity Studies. *Nat. Protoc.* **2010**, *5* (9), 1540–1551.
(28) Songjaroen, T.; Dungchai, W.; Chailapakul, O.; Laiwattanapaisal, W. Novel, Simple and Low-Cost Alternative Method for Fabrication of Paper-Based Microfluidics by Wax Dipping. *Talanta* **2011**, *85* (5), 2587–2593.
(29) Comina, G.; Suska, A.; Filippini, D. Low Cost Lab-on-a-Chip Prototyping with a Consumer Grade 3D Printer. *Lab Chip* **2014**, *14* (16), 2978–2982.
(30) Baker, M. I.; Walsh, S. P.; Schwartz, Z.; Boyan, B. D. A Review of Polyvinyl Alcohol and Its Uses in Cartilage and Orthopedic Applications. *J. Biomed. Mater. Res. B Appl. Biomater.* **2012**, *100B* (5), 1451–1457.
(31) Macdonald, N. P.; Zhu, F.; Hall, C. J.; Reboud, J.; Crosier, P. S.; Patton, E. E.; Wlodkowic, D.; Cooper, J. M. Assessment of Biocompatibility of 3D Printed Photopolymers Using Zebrafish Embryo Toxicity Assays. *Lab Chip* **2016**, *16* (2), 291–297.
(32) Gelber, M. K.; Bhargava, R. Monolithic Multilayer Microfluidics via Sacrificial Molding of 3D-Printed Isomalt†. *Lab Chip* **2015**, *15*, 1736–1741.
(33) Van Midwoud, P. M.; Groothuis, G. M. M.; Merema, M. T.; Verpoorte, E. Microfluidic Biochip for the Perifusion of Precision-Cut Rat Liver Slices for Metabolism and Toxicology Studies. *Biotechnol. Bioeng.* **2010**, *105* (1), 184–194.
(34) Obatomi, D. K.; Brant, S.; Anthonypillai, V.; Early, D. A.; Bach, P. H. Optimizing Preincubation Conditions for Precision-Cut Rat Kidney and Liver Tissue Slices: Effect of Culture Media and Antioxidants. *Toxicol. Vitr.* **1998**, *12* (6), 725–737.

PART II

PAPER SPRAY IONIZATION